Inflammatory Bowel Disease Drivers Revealed in Human Organ Chips

Alican Özkan[1], Gwenn Merry[1], David B. Chou[1,2], Ryan R. Posey[1], Anna Stejskalova[1], Karina Calderon[1], Megan Sperry[1], Viktor Horvath[1,10], Lorenzo E. Ferri[3,4], Emanuela Carlotti[5], Stuart A. C. McDonald[5], Douglas J. Winton[6], Rocco Riccardi[7], Lilianna Bordeianou[7], Sean Hall[1,11], Girija Goyal[1], Donald E. Ingber[1,8,9,*]

[1] Wyss Institute for Biologically Inspired Engineering at Harvard University, Boston, MA
[2] Department of Pathology, Massachusetts General Hospital, Boston, MA
[3] Thoracic and Upper GI Cancer Research Laboratories, Research Institute of McGill University Health Centre, Montreal, QC, Canada
[4] Department of Experimental Surgery and Department of Surgery, McGill University, Montreal, QC, Canada
[5] Clonal Dynamics in Epithelia Laboratory, Queen Mary University of London, London, United Kingdom
[6] Cancer Research UK Cambridge Institute, Li Ka Shing Centre, Cambridge, United Kingdom
[7] Department of Surgery, Massachusetts General Hospital, Boston, MA
[8] Vascular Biology Program and Department of Surgery, Boston Children's Hospital and Harvard Medical School, Boston, MA
[9] Harvard John A. Paulson School of Engineering and Applied Sciences, Cambridge, MA
[10] Current address: Entact Bio, Watertown, MA
[11] Current address: Iovance Therapeutics, Tampa, FL

*Address correspondence to: Donald E. Ingber, MD,PhD
201 Brookline Ave., Suite 401, Boston MA, 02215, USA
em: don.ingber@wyss.harvard.edu

Keywords: Organ-on-a-chip, Ulcerative Colitis, Crohn's Disease, Inflammation, Cancer, Carcinogenesis, Epithelial-Stromal Interactions, Women's health

Abstract

Inflammatory bowel disease (IBD) patients exhibit compromised intestinal barrier function and decreased mucus accumulation, as well as increased inflammation, fibrosis, and cancer risk, with symptoms often being exacerbated in women during pregnancy. Here, we show that these IBD hallmarks can be replicated using human Organ Chips lined by IBD patient-derived colon epithelial cells interfaced with matched fibroblasts cultured under flow. Use of heterotypic tissue recombinants revealed that IBD fibroblasts are the primary drivers of multiple IBD symptoms. Inflammation and fibrosis are accentuated by peristalsis-like motions in IBD Chips and when exposed to pregnancy-associated hormones in female IBD Chips. Carcinogen exposure also increases inflammation, gene mutations, and chromosome duplication in IBD Chips, but not in Healthy Chips. These data enabled by human Organ Chip technology suggest that the intestinal stroma and peristalsis-associated mechanical deformations play a key role in driving inflammation and disease progression in male and female IBD patients.

Main

Inflammation of the intestinal mucosa, including enhanced production of inflammatory cytokines and tissue infiltration with immune cells, along with increased barrier permeability, thinning of the protective mucus layer, and fibrosis are central hallmarks of inflammatory bowel diseases (IBD), such as Crohn's disease (Crohn's) and ulcerative colitis (UC). These alterations lead to significant digestive issues and an increased risk of developing colorectal cancer[1]. IBD symptoms also can be more prominent in women[2] and they have to control their symptoms before pregnancy because exacerbations increase the risk of preterm birth[3]. Most IBD treatments target immune cells rather than intestinal tissues, and treatment efficacy is variable among patients[4]. However, interactions between epithelia and underlying stroma also may

57 contribute to inflammation as well as cancer progression[5]. For example, the presence of a
58 subset of fibroblasts that recruit immune cells to the intestinal stem cell niche is associated with
59 poor prognosis in patients with colorectal cancer[6]. Inflamed epithelial cells also can undergo an
60 epithelial-to-mesenchymal transition and increase deposition of extracellular matrix (ECM)
61 resulting in intestinal fibrosis that leads to complications, such as bowel stiffening and restriction
62 of lumenal fluid flow, which further exacerbate digestive problems in IBD patients [7,8]. Thus, there
63 is a need to gain greater insight into how epithelial-stromal interactions, peristalsis, and fluid
64 flow influence IBD development in both male and female patients. However, animal IBD models
65 and in vitro studies with human intestinal cell lines lack direct relevance to the human disease[9],
66 and human intestinal organoids cannot be used to address these questions because they lack
67 an epithelial-stromal interface, mucosal barrier, fluid flow, peristalsis motions, and immune cells,
68 which are critical organ-level features required to address these questions.
69 Here, we leveraged human organ-on-a-chip (Organ Chip) microfluidic culture technology
70 that recreates tissue-tissue interfaces and a physiologically relevant intestinal microenvironment
71 including dynamic fluid flow, peristalsis-like mechanical deformations, and circulating immune
72 cells to confront this challenge[10,11]. Colon Chips lined by human organoid-derived colonic
73 epithelium cultured under dynamic fluid flow have been successfully used in the past to study
74 mucus layer accumulation and physiology[12,13] as well as to identify microbiome metabolites that
75 influence host response to bacterial infections[14]. In this study, we isolated epithelium and
76 stromal-derived fibroblasts from the same regions of colon from healthy or IBD patients and
77 used them to create Colon Chips that contained an epithelial-fibroblast interface. We also
78 created heterotypic tissue recombinant chips, measured the effects of applying peristalsis-like
79 motions and flowing immune cells through the stromal channel, and studied the effects of
80 female hormones on the IBD state, in addition to modeling cancer progression exposing the
81 Colon Chips to carcinogens in vitro.
82

Results

Establishment of Human Healthy and IBD Colon Chips

Patient-specific epithelial organoids and stromal fibroblasts were isolated from surgical biopsies of the sigmoid colon of healthy and IBD patients with Crohn's or UC (**Extended Data Fig. 1A** and **Supplementary Information**) and the organoids were expanded in Matrigel cultures while the fibroblasts were cultured on plastic dishes (**Extended Data Fig. 1B**). To build the human Colon Chips, the primary colon epithelial cells and fibroblasts were respectively seeded on the top and bottom surfaces of a porous ECM-coated membrane that separates two parallel channels within a commercially available microfluidic Organ Chip (**Fig. 1A**). The cells were allowed to adhere under static conditions for 1 day before flow was initiated. A continuous epithelial monolayer with undulating crypt-like structures formed by 11 days in Healthy Chips when viewed from above (**Fig. 1B,C)** or in cross sections (**Fig. 1D,E**). The epithelium became progressively obscured by dense opaque deposits from day 3 to 7, which completely filled the upper channel by day 11 (**Fig. 1C**). These opaque materials have been shown to be composed of mucus with similar composition, thickness, and bilayer structure as seen in human colonic mucus in vivo [12,13]. Similar chips lined with colonic epithelium and fibroblasts from Crohn's or UC patient samples also formed hill and crypt-like structures, but significantly but significantly less mucus accumulated on top of the epithelium, particularly in the UC chips (**Fig. 1C** and **Extended Data Fig. 1C**) and the heights of the intestinal epithelium were significantly reduced as well (**Fig. 1E**). Epithelial cells within both Healthy and IBD Chips also expressed colon-specific cytokeratin 20 along their apical borders, while the basal stem cell marker SOX9 primarily appeared in their nuclei at the cell base (**Fig. 1F**), which is a hallmark of colon crypts in vivo [23].

Past work has shown that there is a subset of stromal fibroblasts in IBD patients that have higher levels of expression of oncostatin M receptor (OSMR) and podoplanin (PDPN)[6], which appear to play a significant role in inflammation, fibrosis, and cancer[24]. Indeed, when we

109 carried out flow cytometric analysis after removing stromal cells from the chips, we found that
110 PDPN expression was significantly higher in IBD fibroblasts that expressed high OSMR levels
111 (**Extended Data Fig. 2A,B**) and that fibroblasts in IBD Chips lined by cells from both Crohn's
112 and UC patients secreted more inflammatory cytokines (e.g, IL6, IL8, MCP-1) from the basal
113 channel than those in Healthy Chips (**Fig. 1G**). We also found that fibroblasts in IBD Chips
114 established using both Crohn's and UC patients samples express higher vimentin and α-SMA
115 than healthy controls (**Extended Data Fig. 2C,D**), as previously observed in IBD mice models
116 induced by treatment with DSS or IL10 knock out[25].
117 Transcriptomic analysis of epithelial cells and fibroblasts individually within Healthy
118 versus IBD Chips revealed that genes which were found to be overexpressed in Crohn's and
119 UC (e.g., ADA2, APOBEC3B, GSPT2, CD40, ACAN, HLA-DQB1) epithelium on-chip were also
120 expressed at higher levels compared to healthy epithelium (**Extended Data Fig. 3A,B**). In
121 addition, genes suppressed in IBD patient tissues in vivo (e.g., MUC5B, FDFT1 in Crohn's and
122 SOD3, SMIM32, APOBR in UC [26–30]) were expressed at lower levels by epithelium in both
123 Crohn's and UC IBD Chips.
124 When stromal cells cultured in IBD Chips were similarly analyzed, they displayed
125 expression of IBD-relevant genes with Crohn's fibroblasts overexpressing ITGA7, FXD1, HGF,
126 FZD7, NKX2-3, LOXL3 relative to healthy fibroblasts, while high levels of IKBIP, NKX2-3, ADA2,
127 ECM2, NDN, SLC22A17 were seen in UC fibroblasts **(Extended Data. Fig. 3C,D**). In contrast,
128 other genes were downregulated in these fibroblasts including NLRP2, FUCA1, CLCA4, and
129 RNF186 in Crohn's and RALGPS1, DLG3, STON2, and FMO5 in UC derived IBD Chips
130 (**Extended Data Fig. 3C,D**), which is again consistent with results of transcriptomic analyses
131 carried out on IBD patient tissues[31–33].
132 Gene ontology and Reactome analysis revealed that multiple IBD-relevant biological
133 processes, including increased ECM production and remodeling, cell adhesion, and
134 angiogenesis as well as decreased metabolism were predominant in both Crohn's and UC

135 epithelium and fibroblasts on-chip, with UC tissues also exhibiting suppressed IL10 signaling
136 (**Extended Data Fig. 4A-D**). These functional pathways are also activated or suppressed in a
137 similar manner in IBD patients[34].

138 **Peristalsis-Like Mechanical Motions Enhance IBD Progression**

139 IBD patients experience thinning of the protective mucus layer in their colon[12] and
140 eventually loss of peristalsis as a consequence of increased fibrosis[7,8], which further exacerbate
141 their gastrointestinal symptoms. However, it is not known whether cyclic mechanical
142 deformation of inflamed intestine or fluid flow due to peristalsis could influence IBD disease
143 progression. To explore this possibility, we cultured Healthy and IBD Chips in the presence or
144 absence of physiologically relevant cyclic deformations by applying suction to side chambers in
145 the flexible devices. The healthy and IBD epithelia both accumulated a mucus layer when
146 exposed to cyclic mechanical deformations were viewed by dark field imaging; however, the
147 layer was much thinner in the IBD Chips (**Fig. 2A,B**). Transcriptomic analysis confirmed that the
148 IBD Chips expressed lower levels of most mucins than Healthy Chips under all conditions, and
149 that while expression of MUC-1,4,12,13,17,3A,5AC, and 5B increased in Healthy Chips
150 exposed to mechanical strain, only MUC5AC and MUC13 increased in the IBD Chips (**Fig. 2C)**.
151 These data show that peristalsis-like mechanical deformations have a direct effect on mucus
152 production in the colonic epithelium in both healthy and IBD Chips as fluid flow was constant
153 under all conditions, and that the IBD epithelium is less effective at maintaining the normal
154 thickness of the mucus layer in vitro as observed in IBD patients in vivo[12,13].

155 Interestingly, second harmonic imaging of ECM fiber formation on-chip revealed that
156 while both Crohn's and UC derived IBD fibroblasts accumulate comparable fibrillar collagen as
157 healthy cells, these levels increase many fold when the IBD Chips are exposed to peristalsis-
158 like motions whereas there is no change in Healthy Chips (**Fig. 2D,E**). Atomic force
159 microscopic analysis carried out in parallel samples from the biopsies we used to isolate the
160 patient-derived cells confirmed that this was associated with tissue stiffening (**Extended Data**

161 **Fig. 5A-D**). But while transcriptomic analysis showed that there is increased expression of
162 collagen-associated genes in Crohn's and UC stroma on-chip without mechanical strain,
163 exposure to peristalsis-like deformations did not result in significant changes in collagen gene
164 expression (**Fig. 2F**), suggesting that the fibrotic changes we observed resulted from post-
165 transcriptional alterations. Indeed, pathway analysis confirmed that biological processes
166 associated with fibrosis per se (ECM organization, collagen formation and fibril organization)
167 were upregulated in IBD Chips upon exposure to cyclic mechanical deformations (**Extended**
168 **Fig. 6A**). In addition, our transcriptomic analysis revealed that expression of different
169 cytochrome P450 subunits was suppressed in IBD versus Healthy Chips, which is consistent
170 with the observation that the intestinal tissues of IBD patients experience decreased metabolic
171 activities[35,36]. Importantly, while peristalsis-like cyclic deformations increased the expression of
172 most of these metabolic genes in Healthy Chips, this response was not observed in IBD Chips
173 (**Extended Data Fig. 6B**).
174 Peristalsis-like cyclic deformations also increased barrier function in both Healthy and
175 IBD Chips; however, barrier leakiness always remained higher in IBD Chips (**Extended Data**
176 **Fig. 7A**). Mechanical stimulation also enriched expression of inflammation associated genes in
177 epithelial cells and fibroblasts in both Healthy and IBD Chips (**Fig. 2G**) and this was supported
178 by transcriptomic analysis, which showed activation of the inflammatory response pathway in
179 these cells (**Extended Data Fig. 7B**). Importantly, further pathway analysis of this transcriptomic
180 dataset (**Extended Data Fig. 8**) demonstrated that peristalsis-like deformations activate
181 pathways associated with IBD progression and exacerbation in the epithelium, including those
182 involved in cancer, Toll-like receptor signaling, PPAR signaling, and focal adhesion in IBD
183 epithelium (**Extended Data Fig. 9A**) as well as NOD-like receptor signaling, PDGF signaling,
184 and cytokine-cytokine receptor interaction in IBD fibroblasts (**Extended Data Fig. 9B**). In
185 contrast, these pathways that are known to exacerbate colitis in IBD patients[37,38] were not
186 activated in Healthy Chips under the same mechanical stimulation conditions.

187 **Replicating Sex-Specific Clinical Symptoms of IBD Patients**

188 The gastrointestinal symptoms of female IBD patients become much more prominent
189 during menstrual periods[2] and their therapies need to be optimized to control their symptoms
190 before pregnancy due to increased risk to the fetus[3]. Yet, it is not known whether these
191 responses are a direct effect of ovarian hormones on the intestine[39]. To address this question
192 directly, we exposed healthy and IBD Chips lined by cells from female patients to estrogen (E2)
193 and medroxyprogesterone acetate (MPA) to recapitulate the menstrual cycle or a mixture of
194 pregnancy-associated hormones (E2, MPA, human chorionic gonadotropin, prolactin, and
195 placental lactogen) to mimic the first trimester of pregnancy. Interestingly, exposure to E2, MPA
196 or the pregnancy-associated hormone mixture decreased inflammatory cytokine and chemokine
197 production in Healthy Chips whereas levels of these inflammatory molecules increased when
198 IBD Chips were exposed to the same hormones (**Fig. 3A).** Moreover, addition of E2 and MPA
199 increased fibrosis and exposure to the pregnancy-associated hormone mixture produced an
200 even greater increase in fibrillar collagen deposition in the stroma of IBD Chips; however, this
201 was not observed in Healthy Chips (**Fig. 3B,C).**

202 **Stromal Fibroblasts Control Barrier Permeability and Epithelial Inflammation**

203 To better understand the role of fibroblasts in IBD, we took advantage of the synthetic
204 biology nature of human Organ Chip technology to create chips lined by heterotypic tissue
205 recombinants of healthy epithelium with IBD stroma and vice versa. As expected, the homotypic
206 cultures of IBD epithelium and stroma had a compromised barrier with higher permeability than
207 healthy epithelium and stroma recombinants (**Fig. 4A**). However, we discovered that the
208 presence of the IBD fibroblasts was the key driver of barrier disruption as permeability increased
209 significantly when they were combined healthy epithelium in tissue recombinant chips, even
210 though there was no difference in permeability when the different epithelia were cultured alone
211 (**Fig. 4A)**. Interestingly, the permeability of the IBD epithelium alone (i.e., without IBD stroma)
212 was similar to that of healthy epithelium with or without healthy fibroblasts, and tissue

213 recombinants combining healthy fibroblasts with IBD epithelium also did not further alter barrier
214 function, again emphasizing the key role of that the IBD stroma plays in terms of compromising
215 intestinal barrier function.

216 This controlling effect of IBD fibroblasts on barrier function when combined with healthy
217 epithelium was also accompanied by increased production of multiple inflammatory cytokines
218 and chemokines including IL-6, MCP-1 (**Fig. 4B**), IL-8, CXCL-1, LIF, IL-21, PIGF-1, and MIP-1b
219 (**Extended Data Fig. 10A**) relative to chips lined by healthy fibroblasts and epithelium or healthy
220 epithelium alone. However, the IBD epithelium appeared to constitutively express high levels of
221 all these cytokines regardless of whether or not IBD fibroblasts were present or they were
222 replaced with healthy fibroblasts, except for production of IL-6 and MCP-1 that were further
223 enhanced by the presence of the IBD stroma (**Fig. 4C** and **Extended Data Fig. 10B**). As these
224 two cytokines are known to promote monocyte infiltration into stroma from the vascular system
225 and their differentiation to macrophages cells[40], we perfused human peripheral blood
226 mononuclear cells (PBMCs) through the basal channel of the Colon Chips. We found that more
227 PBMCs adhered to the stroma and migrated to the epithelial channel in the IBD Chips
228 compared to Healthy Chips (**Fig. 4D**). While application of peristalsis-like deformations did not
229 alter PBMC adhesion to the stroma in the basal channel, it significantly enhanced the migration
230 of these cells to the epithelium in the apical channel, but only in IBD Chips (**Fig. 4E**). However,
231 when we carried out a similar study in a heterotypic tissue recombinant chip containing IBD
232 epithelium with healthy fibroblasts, PBMC recruitment and migration were suppressed and
233 reverted to the low levels observed in Healthy Chips (**Fig. 4D,E**). This finding correlates well
234 with transcriptomic analysis, which revealed that multiple surface receptors for immune cell
235 adhesion are expressed at higher levels in fibroblasts and epithelium in IBD Chips versus
236 Healthy Chips (**Extended Data Fig. 10C**). IBD Chips co-cultured with PBMCs also showed
237 increased production of IL-6 and IL-8 in both their apical and basal channels, whereas this was
238 not observed when Healthy Chips (**Extended Data Fig. 10D**).

239 **Modeling Early Cancer Progression in Human IBD Chips**

240 Patients with IBD have a higher incidence of colorectal cancer formation[41] and this also
241 has been demonstrated in animal IBD models by exposing them to the carcinogen ENU[42].
242 When we exposed Healthy and IBD Chips created with cells from multiple different donors to
243 ENU (1 mM) for 3 weeks, we observed a decrease in the height of crypt-like structures (**Fig.**
244 **5A,B**) and an increase in barrier permeability (**Fig. 5C**) in both in healthy and IBD Chips.
245 However, ENU had a much greater impact on inflammatory cytokine secretion in the IBD Chips
246 (**Fig. 5D**) and it resulted in a greater reduction of E-cadherin expression in IBD Chips versus
247 Healthy Chips, which was accompanied by a concomitant increase in β-catenin translocation to
248 the nucleus (**Fig. 5E,F**). Similar activation of the β-catenin signaling pathway has previously
249 been shown to be associated with colorectal cancer progression[43]. In addition, ENU treatment
250 promoted enlargement of epithelial nuclei and a decrease in their roundness, which are also
251 known to accompany early carcinogenesis[44]. Importantly, shallow pass genome sequencing
252 revealed increased gene mutations and duplication in IBD Chips, but not in Healthy Chips (**Fig.**
253 **5G**). Interestingly, the Crohn's chips exhibited a higher level of gene amplification than chips
254 lined with cells from UC patients, and an existing mutation in one Crohn's patient was further
255 amplified after ENU exposure.

256

257 **Discussion**

258 Taken together, these findings show that human Colon Chips created with primary
259 patient-derived colonic epithelium and fibroblasts from both healthy and IBD patients
260 recapitulate many features of their respective healthy and diseased phenotypes that are
261 observed in vivo. Based on its synthetic nature, this model enabled exploration of the roles of
262 stromal fibroblasts, epithelium, and immune cells, as well as fluid flow and peristalsis-like
263 mechanical deformations in the etiology of this disease. Importantly, our results revealed that

264 the stroma is a key driver of the IBD phenotype as it is appears to drive effects on intestinal
265 permeability, inflammation, and immune cell infiltration in human intestinal tissues. The finding
266 that IBD stromal fibroblasts respond differently to physiological peristalsis motions than healthy
267 fibroblasts and exhibits enhanced inflammation and fibrotic responses while fluid flow was
268 maintained constant also suggests that physiological mechanical deformations of intestine
269 during early stages of IBD development may feed back to further enhance inflammation and
270 fibrosis thereby accelerating disease progression. In addition, we found that ovarian hormones
271 influence the IBD phenotype directly by targeting the intestinal stroma. The greater
272 enhancement of inflammation and fibrosis we observed when IBD Chips were exposed to these
273 female hormones could be at least in part explain the exacerbation of IBD symptoms observed
274 in women versus men, particularly during pregnancy. Finally, we demonstrated that the human
275 IBD Chips also exhibit an enhanced sensitivity to a carcinogen and undergo changes that
276 underlie early stages of carcinogenesis in vitro, which is again consistent with the finding that
277 IBD patients have an increased propensity to develop colorectal cancers.
278 Our finding that intestinal stromal fibroblasts influence immune cell trafficking is
279 consistent with a past study in which knock out of genes expressed in an inflammatory subset of
280 fibroblasts produced a similar effect in a mice DSS colitis model[12]. These results raise the
281 possibility that human Colon Chips could be used as a preclinical model with IBD patient cells to
282 study the effects of emerging immune cell targeting therapies (e.g., anti-integrin $\alpha 4\beta 7$ to
283 suppress infiltration of circulating T-cells) on IBD stroma versus epithelium and to determine
284 their potential efficacy in a patient-specific manner[45]. In addition, this work might serve as
285 inspiration to develop other stroma-targeted therapies given our findings that the stroma is a key
286 driver of the IBD state in both females and males. The stroma also plays a critical role in
287 intestinal homeostasis by supporting the intestinal stem cell niche growth and modulating
288 immune responses, as well as protection against microbiota[46].

289 Another novel feature of this study is its relevance for Women's Health. Female IBD patients
290 can experienced loose and increased stools during the menstrual cycle as well as greater fetal
291 complications during pregnancy [39,47]. However, it has not been possible in the past to explore
292 whether or not these symptoms are the result of direct effects of female hormones on intestinal
293 tissues. This is because female hormone research is challenging using animals. For example,
294 mice that are often used for women's health research[48] do not menstruate like humans do (e.g.,
295 they undergo an estrous cycle) and their immune responses different significantly from human[49].
296 Consistent with clinical observations, we found that female hormones exacerbate inflammation
297 and fibrosis in IBD Chips, but not in Healthy Chips, with pregnancy-like conditions producing
298 even greater effects. Thus, these data demonstrate for the first time that at least part of the
299 excerbations observed in female patients is likely due to direct effects on the intestinal tissues,
300 and particular on the stroma where fibrosis is greatly enhanced.
301 In addition to increased inflammation and decreased mucus production, lack of intestinal
302 motion due to fibrosis is a hallmark of IBD; however, it has not been previously possible to
303 explore whether peristalsis plays a role in earlier stages of IBD progression. We found that
304 peristalsis-like mechanical deformations increased production of the protective mucus layer in
305 Healthy Chips, but less so in IBD Chips, and that these mechanical cues also enhanced
306 inflammation and fibrosis, but only in IBD Chips. This suggests that persistence of physiological
307 peristalsis during early stages of inflammation may promote progression of IBD, and that fibrosis
308 and resultant suppression of peristalsis likely occur at a later stage in this process. This may, in
309 part, occur because the IBD tissues lose their ability to maintain the mucus barrier that protects
310 against dysbiotic microbiome and pathogens that are known to be enriched in the microbiome of
311 IBD patients, such as *Ruminococcus* family members that degrade mucus[50]. This could then
312 lead to more inflammation and a positive feedback loop characterized by enhanced sensitivity to
313 these mechanical deformations resulting in greater increases in inflammation, ECM

314 accumulation, and fibrosis at later stages of the disease, which stiffens the mucosa and
315 physically restricts tissue distension.[41]
316 Chronic inflammation in patients with IBD is known to be a risk factor for increased cancer
317 formation. Importantly, our results show that human IBD tissues do indeed exhibit an enhanced
318 sensitivity to a carcinogen (ENU) compared to Healthy colon tissues on-chip, as indicated by
319 crypt blunting, loss of adherent junctions, and localization of β-catenin to the nucleus as seen in
320 IBD patient tissues that progressed to colorectal cancer[51]. Importantly, we also observed a
321 greatly increased inflammatory response as well as accelerated development of cancer-
322 associated mutations and chromosomal amplifications in IBD Chips but not Healthy Chips, even
323 though immune cells were not present. While similar effects have been observed after exposure
324 to ENU in a murine intestine model [52], this to our knowledge is the first demonstration of early
325 cancer progression in a preclinical *human* IBD model. Although it has been believed that both
326 Crohn's and UC patients carry a similarly high risk of cancer progression [53], many Crohn's
327 patients undergo colectomy early in the course of the disease to alleviate persistent
328 symptoms[54], and this effectively eliminates their risk of developing colorectal cancer.[59]
329 Interestingly, although our sampling was small, we found that ENU induced greater gene and
330 chromosomal aberrations in Crohn's patient tissues than in UC patient chips, suggesting that
331 they might exhibit a greater susceptibility to carcinogens. This is a finding which should be
332 followed up in clinical studies in the future.
333 The incidence of IBD is anticipated to increase in the upcoming years. Limitations in the
334 ability of in vivo models to represent human IBD physiology are evident, as the most commonly
335 used anti-TNF and anti-IL-12/23p40 antibodies, which benefit patients with IBD, are generally
336 not effective in chemically-induced colitis models[55]. The need for modeling IBD using Organ
337 Chip technology also has been acknowledged by leading IBD organizations, such as the
338 Crohn's and Colitis Foundation[56]. Therefore, we believe this novel microfluidic disease model
339 brings important opportunities for IBD treatment, management, and drug development. As we

340 can analyze outflows from the epithelial and stromal compartments separately and through use
341 of tissue recombinants, this method also may facilitate discovery of potential stool and blood
342 biomarkers of IBD progression and cancer risk. Use of tissue recombinants is a powerful
343 method for analyzing epithelial-mesenchymal interactions in commonly used developmental
344 biology research, which as we show here also may be applied to confront similar questions
345 relating to human epithelial-stromal interactions, which are challenging to address in vivo. In
346 addition to enabling study of the effects of female hormones on IBD, and it also could allow
347 investigation of other IBD subcategories, including very early onset (VEO-IBD), adolescent IBD,
348 and genetic forms of the disease by lining chips with relevant patient cells. Finally, given the
349 synthetic nature of the model and as living gut microbiome can be co-cultured in these Intestine
350 Chips for extended times[15,57], this experimental system also may be used to study how other
351 environmental factors (e.g., pathogens, diet, etc.) contribute to development of the IBD
352 phenotype in the future.

353 **Methods**

354 **Acquisition of human colon tissue and cells**

355 Healthy colon tissue samples were collected from macroscopically grossly unaffected
356 regions of the colon of de-identified healthy adult patients undergoing endoscopy for non-IBD
357 related complaints, such as diverticulitis. IBD tissue samples were collected from endoscopic
358 tissue biopsies from newly diagnosed IBD patients with either Crohn's disease or Ulcerative
359 Colitis. Informed consent and developmentally appropriate assent were obtained at Boston
360 Children's Hospital and McGill University Health Centre from the donors' guardians and the
361 donor, respectively. All methods were performed in accordance with the Institutional Review
362 Board of Massachusetts General Hospital approval (protocol number IRB-2015P001859) and
363 McGill University Health Centre (protocol number REB-2007-856). We generated epithelium-
364 derived organoids (colonoids) that were cultured in Matrigel using published methods[13,15]and
365 isolated stromal fibroblasts from the same IBD tissues from 3 Crohn's and 3 UC patients, which

366 were cultured in fibroblast medium (FM, CC-3132, Lonza, MA) in 75 cm^2 flasks (3531135,
367 Falcon, Durham, NC). Healthy colonoids and fibroblasts were isolated from areas with normal
368 histology adjacent to regions of diverticulitis from 3 otherwise healthy patients (**Supplementary**
369 **Table 1**). All reagents and resources were provided in **Supplementary Table 2**.

370 **Human Colon Chip Cultures**

371 Our methods for creating and culturing human Colon Chips lined by primary intestinal
372 organoid-derived epithelium using commercially available Organ Chip Devices (Basic Research
373 Kit; Emulate Inc.) have been described previously[13,16] and are described in greater detail in
374 Supplementary Materials. Colonoids cultured were released from Matrigel and fragmented by
375 treatment with TrypLE Express Enzyme (12605010; Thermo Fisher Scientific), before being
376 seeded in the apical channel of the 2-channel Organ Chip devices and incubated overnight at
377 37° C under 5% CO_2 to promote adhesion. One day later, channels were washed with
378 Expansion Medium (EM; Harvard Digestive Diseases Center Organoid Core, MA) to remove
379 unattached cells, and then perfused with EM (60 µL/hr). At this time, the cultured fibroblasts
380 were detached enzymatically and seeded in EM in the basal channel for 2 h under static
381 conditions to promote adhesion. After washing, EM was then perfused through both channels at
382 60 µL/h. After 3 days of co-culture during which both epithelial and fibroblast monolayers were
383 established, EM perfused through the apical channel was changed to Hank's balanced salt
384 solution (HBSS) with calcium and magnesium (21-023-cv; Corning) supplemented with 100
385 mg/mL Primocin (ant-pm-1; InvivoGen) while EM remained flowing through the basal channel.
386 For experiments exploring the role of physiological peristalsis-like motions, cyclic mechanical
387 strain (10% Strain 0.15 Hz) was applied to the tissues by applying cyclic suction to side
388 chambers of the flexible device[15,16] for 2 weeks after seeding. Methods for morphological
389 analysis, cytokine quantification, flow cytometry, transcriptional analysis, and atomic force
390 microscopy can be found in **Supplementary Information**.

391 **Maternal Hormone Treatment**

392 Established Healthy and IBD Colon Chips were exposed to different combinations of
393 hormones from basal channel to recapitulate either the menstrual cycle or first trimester of
394 pregnancy. Chips were treated with 17β-estradiol (E2, 10 nM, Sigma, E4389) for 3 days before
395 being exposed to medroxyprogesterone 17-acetate (MPA, 1 μM, Sigma, 46412-250MG) for an
396 additional 4 days to mimic the menstrual period of the cycle. Chips perfused for 3 days with E2
397 were then treated with E2, MPA, Prolactin (PRL, 20 ng/mL, VWR, 103681-334), Human
398 Placental Lactogen (hPL/ CSH1, 20 ng/ml, VWR, 103681-334), and Human Chorionic
399 Gonadotropin (HCG, 1 μg/mL, VWR, IC0219859110) for 4 days to recapitulate the first trimester
400 of pregnancy as described previously[17,18].

401 **Immune Cell Recruitment Assay**

402 Colon Chips were cultured for 2 weeks before human peripheral blood mononuclear
403 cells (PBMCs) were added to the cultures for studies on immune cell adhesion and migration.
404 PBMCs were collected from anonymous donors undergoing stem cell mobilization at the
405 Massachusetts General Hospital (MGH) under Institutional Review Board approved protocol
406 #2015P001859. PBMCs were freshly isolated by density centrifugation using the Lymphoprep
407 protocol (StemCell Technologies, #07801), resuspended in 10 ml of DMEM containing 10%
408 FBS and 1% Penicillin-Streptomycin, and labeled with 10 μl of CellTracker Deep Red at a final
409 concentration of 10 μM (Invitrogen, #C7025) for 20 minutes at 37°C. The labeled cells were
410 centrifuged and resuspended to a concentration of 5×10^7 cells/ml and 25 μl of the PBMC
411 suspension was added to the lower channel (see **Supplementary Information** for more
412 details).

413 **Analysis of effects of carcinogen exposure**

414 To explore if the chip models can be used to study the effects of intestinal tissue to
415 carcinogen exposure in vitro, Healthy and IBD Colon Chips were exposed to 1 μg/mL of N-ethyl-
416 N-nitrosourea (ENU), which was flowed through both the apical and basal channels at 60 μL/hr.

417 Chips were harvested for DNA isolation three weeks after ENU exposure. Briefly, chips were
418 washed with DPBS (-/-) and incubated with TrypLE consisting of 2 mg/mL collagenase and 10
419 μM Y-27632 at 37ºC for 1 h. Single cells were washed with DPBS (-/-) and DNA was isolated by
420 following the manufacturer's protocol (Qiagen Micro DNA isolation kit, Cat: 56304 Qiagen,
421 Germany). Shallow whole genome sequencing was performed in two batches using different
422 methods (see **Supplementary Information**). The raw sequence reads were mapped to *Homo*
423 *sapiens* GRCh38 with Burrows-Wheeler Alignment Tool v0.7.17[19]. Reads with a mapping quality
424 of less than 37 were removed from further analysis. The PCR duplicates and base quality
425 recalibration were subsequently carried out using Genome Analysis Toolkit (GATK) v4.4.0[20] and
426 Picard v2.27.5. The copy number of the genome was then estimated and profiled with ACE
427 v3.16[21] and QDNAseq v1.35.0 R package[22] using 100 Mb fixed-sized bins.

428 **Statistical Analysis**

429 Data in all graphs are expressed as mean ± standard deviation (SD) and significant
430 differences between multiple groups were determined using an unpaired Students t-test, one-
431 way analysis of variance (ANOVA) or two-way ANOVA with Tukey test for correction unless
432 otherwise indicated in the figure legends. $P<0.05$ was considered significant. Data were
433 analyzed using GraphPad Prism 8 software (GraphPad Software, San Diego, CA).

434 **Acknowledgement**

435 This work was funded in part by Cancer Research UK (C19767/A27145 to DEI) and by
436 the Wyss Institute for Biologically Inspired Engineering at Harvard University as well as by an
437 NIH training grants (5T32DK007199-44 and 5T32EB016652-10 to AO). We thank Harvard
438 Digestive Diseases Center Organoid Core for providing L-WRN conditioned media.

439 **Contributions**

440 A.O., S.H. and D.E.I designed the research; A.O., G.E.M, R.R.P. A.S. K. C., E. C. performed the
441 experiments; A.O., G.E.M., R.R.P. A.S., K.C., E.C. analyzed and interpreted the data; A.O. and
442 G.E.M. established IBD human organoid and fibroblast biobanks; V. H., M. S. and A.O.

443 performed bioinformatic analysis; D.B.C., L.E.F., R.R., L.B. provided the clinical samples; A.O.
444 and D.E.I. acquired the funding; A.O. wrote the articled with input from G.G., S.H. and D.E.I.;
445 and all authors reviewed, discussed and edited the manuscript.

446 **Data and code availability**

447 Data that support the findings of this study are available within the paper and its
448 Supplementary Information files. The RNA sequencing data have been deposited in the Gene
449 Expression Omnibus (GEO) with the accession code GSE277964. Any other material including
450 the R code used for data analysis is available upon reasonable request.

451 **Competing interests**

452 D.E.I. holds equity in Emulate, chairs its scientific advisory board and is a member of its board
453 of directors. The other authors declare no competing interests.

454 ## References

455 1. Friedrich, M. *et al.* IL-1-driven stromal–neutrophil interactions define a subset of patients
456 with inflammatory bowel disease that does not respond to therapies. *Nat Med* **27**, 1970–
457 1981 (2021).
458 2. Goodman, W. A., Erkkila, I. P. & Pizarro, T. T. Sex matters: impact on pathogenesis,
459 presentation and treatment of inflammatory bowel disease. *Nature Reviews*
460 *Gastroenterology & Hepatology 2020 17:12* **17**, 740–754 (2020).
461 3. Watermeyer, G. Pregnancy and inflammatory bowel disease. *South African*
462 *Gastroenterology Review* **5**, 4–6 (2007).
463 4. Sarvestani, S. K. *et al.* Cancer-predicting transcriptomic and epigenetic signatures
464 revealed for ulcerative colitis in patient-derived epithelial organoids. *Oncotarget* **9**,
465 28717–28730 (2018).
466 5. Ingber, D. E. Cancer as a disease of epithelial–mesenchymal interactions and
467 extracellular matrix regulation. *Differentiation* **70**, 547–560 (2002).
468 6. Smillie, C. S. *et al.* Intra- and Inter-cellular Rewiring of the Human Colon during Ulcerative
469 Colitis. *Cell* **178**, 714-730.e22 (2019).
470 7. Rieder, F. & Fiocchi, C. Intestinal fibrosis in IBD - A dynamic, multifactorial process. *Nat*
471 *Rev Gastroenterol Hepatol* **6**, 228–235 (2009).

472 8. Guglielmo, F. F. *et al.* Identifying decreased peristalsis of abnormal small bowel
473 segments in Crohn's disease using cine MR enterography: the frozen bowel sign. *Abdom*
474 *Imaging* **40**, 1150–1156 (2015).
475 9. Joshi, A., Soni, A. & Acharya, S. In vitro models and ex vivo systems used in
476 inflammatory bowel disease. *In vitro models 2022 1:3* **1**, 213–227 (2022).
477 10. Özkan, A., LoGrande, N. T., Feitor, J. F., Goyal, G. & Ingber, D. E. Intestinal organ chips
478 for disease modelling and personalized medicine. *Nat Rev Gastroenterol Hepatol* 1–23
479 (2024) doi:10.1038/s41575-024-00968-3.
480 11. Ingber, D. E. Human organs-on-chips for disease modelling, drug development and
481 personalized medicine. *Nat Rev Genet* **23**, 467–491 (2022).
482 12. Gustafsson, J. K. & Johansson, M. E. V. The role of goblet cells and mucus in intestinal
483 homeostasis. *Nat Rev Gastroenterol Hepatol* **19**, 785–803 (2022).
484 13. Sontheimer-Phelps, A. *et al.* Human Colon-on-a-Chip Enables Continuous In Vitro
485 Analysis of Colon Mucus Layer Accumulation and Physiology. *Cmgh* **9**, 507–526 (2020).
486 14. Tovaglieri, A. *et al.* Species-specific enhancement of enterohemorrhagic E. coli
487 pathogenesis mediated by microbiome metabolites. *Microbiome* **7**, 1–21 (2019).
488 15. Jalili-Firoozinezhad, S. *et al.* A complex human gut microbiome cultured in an anaerobic
489 intestine-on-a-chip. *Nat Biomed Eng* **3**, 520–531 (2019).
490 16. Tovaglieri, A. *et al.* Species-specific enhancement of enterohemorrhagic E. coli
491 pathogenesis mediated by microbiome metabolites. *Microbiome* **7**, 1–21 (2019).
492 17. Turco, M. Y. *et al.* Long-term, hormone-responsive organoid cultures of human
493 endometrium in a chemically defined medium. *Nat Cell Biol* **19**, 568–577 (2017).
494 18. Gnecco, J. S. *et al.* Organoid co-culture model of the human endometrium in a fully
495 synthetic extracellular matrix enables the study of epithelial-stromal crosstalk. *Med* **4**,
496 554-579.e9 (2023).
497 19. Li, H. & Durbin, R. Fast and accurate short read alignment with Burrows–Wheeler
498 transform. *Bioinformatics* **25**, 1754–1760 (2009).
499 20. Genomics in the Cloud: Using Docker, GATK, and WDL in Terra - Geraldine A. Van der
500 Auwera, Brian D. O'Connor - Google Books.
501 https://books.google.com/books?hl=en&lr=&id=vsXaDwAAQBAJ&oi=fnd&pg=PP1&dq=V
502 an+der+Auwera+GA+%26+O%27Connor+BD.+(2020).+Genomics+in+the+Cloud:+Using
503 +Docker,+GATK,+and+WDL+in+Terra+(1st+Edition).+O%27Reilly+Media.&ots=5lcr0E-
504 qna&sig=43MTbQQNO_yexxB7NxDgVt88kOk#v=onepage&q&f=false.

505 21. Poell, J. B. *et al.* ACE: absolute copy number estimation from low-coverage whole-
506 genome sequencing data. *Bioinformatics* **35**, 2847–2849 (2019).
507 22. Scheinin, I. *et al.* DNA copy number analysis of fresh and formalin-fixed specimens by
508 shallow whole-genome sequencing with identification and exclusion of problematic
509 regions in the genome assembly. *Genome Res* **24**, 2022–2032 (2014).
510 23. Chan, C. W. M. *et al.* Gastrointestinal differentiation marker Cytokeratin 20 is regulated
511 by homeobox gene CDX. *Proc Natl Acad Sci U S A* **106**, 1936–1941 (2009).
512 24. West, N. R. *et al.* Oncostatin M drives intestinal inflammation and predicts response to
513 tumor necrosis factor–neutralizing therapy in patients with inflammatory bowel disease.
514 *Nat Med* **23**, 579–589 (2017).
515 25. Wu, J. *et al.* Therapeutic targeting of vimentin by ALD-R491 impacts multiple pathogenic
516 processes to attenuate acute and chronic colitis in mice. *Biomedicine & Pharmacotherapy*
517 **168**, 115648 (2023).
518 26. Torres, J. *et al.* Serum Biomarkers Identify Patients Who Will Develop Inflammatory
519 Bowel Diseases Up to 5 Years Before Diagnosis. *Gastroenterology* **159**, 96–104 (2020).
520 27. Danese, S., Sans, M. & Fiocchi, C. The CD40/CD40L costimulatory pathway in
521 inflammatory bowel disease. *Gut* **53**, 1035 (2004).
522 28. Liu, Z. *et al.* Genetic architecture of the inflammatory bowel diseases across East Asian
523 and European ancestries. *Nat Genet* **55**, 796 (2023).
524 29. Tian, T., Wang, Z. & Zhang, J. Pathomechanisms of Oxidative Stress in Inflammatory
525 Bowel Disease and Potential Antioxidant Therapies. *Oxid Med Cell Longev* **2017**,
526 4535194 (2017).
527 30. Stokkers, P. C. F., Reitsma, P. H., Tytgat, G. N. J. & Van Deventer, S. J. H. HLA-DR and
528 -DQ phenotypes in inflammatory bowel disease: a meta-analysis. *Gut* **45**, 395 (1999).
529 31. Yu, W. *et al.* Association of a Nkx2-3 polymorphism with Crohn's disease and expression
530 of Nkx2-3 is up-regulated in B cell lines and intestinal tissues with Crohn's disease. *J*
531 *Crohns Colitis* **3**, 189–195 (2009).
532 32. WO2019018571A1 - Methods and uses of inflammatory bowel disease biomarkers -
533 Google Patents. https://patents.google.com/patent/WO2019018571A1/en.
534 33. Srivastava, M., Zurakowski, D., Cheifetz, P., Leichtner, A. & Bousvaros, A. Elevated
535 Serum Hepatocyte Growth Factor in Children and Young Adults With Inflammatory Bowel
536 Disease. *J Pediatr Gastroenterol Nutr* **33**, 548–553 (2001).

537 34. Cheng, C. *et al.* Identification of differentially expressed genes, associated functional
538 terms pathways, and candidate diagnostic biomarkers in inflammatory bowel diseases by
539 bioinformatics analysis. *Exp Ther Med* **18**, 278–288 (2019).
540 35. Wilson, A. *et al.* Crohn's Disease Is Associated with Decreased CYP3A4 and P-
541 Glycoprotein Protein Expression. *Mol Pharm* **16**, 4059–4064 (2019).
542 36. Sen, A. & Stark, H. Role of cytochrome P450 polymorphisms and functions in
543 development of ulcerative colitis. *World J Gastroenterol* **25**, 2846 (2019).
544 37. Dubuquoy, L. *et al.* PPARγ as a new therapeutic target in inflammatory bowel diseases.
545 *Gut* **55**, 1341 (2006).
546 38. Ashton, J. J. *et al.* Deleterious Genetic Variation Across the NOD Signaling Pathway Is
547 Associated With Reduced NFKB Signaling Transcription and Upregulation of Alternative
548 Inflammatory Transcripts in Pediatric Inflammatory Bowel Disease. *Inflamm Bowel Dis*
549 **28**, 912–922 (2022).
550 39. Lim, S. M. *et al.* The effect of the menstrual cycle on inflammatory bowel disease: A
551 prospective study. *Gut Liver* **7**, 51–57 (2013).
552 40. Chomarat, P., Banchereau, J., Davoust, J. & Karolina Palucka, A. IL-6 switches the
553 differentiation of monocytes from dendritic cells to macrophages. *Nature Immunology*
554 *2000 1:6* **1**, 510–514 (2000).
555 41. Murphy, C. C. & Zaki, T. A. Changing epidemiology of colorectal cancer — birth cohort
556 effects and emerging risk factors. *Nat Rev Gastroenterol Hepatol* **21**, 25–34 (2023).
557 42. Schmitt, M. & Greten, F. R. The inflammatory pathogenesis of colorectal cancer. *Nat Rev*
558 *Immunol* **21**, 653–667 (2021).
559 43. Herzig, M., Savarese, F., Novatchkova, M., Semb, H. & Christofori, G. Tumor progression
560 induced by the loss of E-cadherin independent of β-catenin/Tcf-mediated Wnt signaling.
561 *Oncogene* **26**, 2290–2298 (2007).
562 44. Zink, D., Fischer, A. H. & Nickerson, J. A. Nuclear structure in cancer cells. *Nature*
563 *Reviews Cancer 2004 4:9* **4**, 677–687 (2004).
564 45. D'Alessio, S. *et al.* Revisiting fibrosis in inflammatory bowel disease: the gut thickens. *Nat*
565 *Rev Gastroenterol Hepatol* **19**, 169–184 (2022).
566 46. Ryan, F. J. *et al.* Colonic microbiota is associated with inflammation and host epigenomic
567 alterations in inflammatory bowel disease. *Nat Commun* **11**, 1–12 (2020).
568 47. Mendelson, S., Anbukkarasu, P., Cassisi, J. E. & Zaman, W. Gastrointestinal functioning
569 and menstrual cycle phase in emerging young adult women: a cross-sectional study.
570 *BMC Gastroenterol* **23**, 1–10 (2023).

48. Bellofiore, N., Ellery, S., Mamrot, J., … D. W.-A. journal of & 2017, undefined. First evidence of a menstruating rodent: the spiny mouse (Acomys cahirinus). *Elsevier*.
49. Bellofiore, N., Cousins, F., Temple-Smith, P., Dickinson, H. & Evans, J. A missing piece: the spiny mouse and the puzzle of menstruating species. *J Mol Endocrinol* **61**, R25–R41 (2018).
50. Paone, P. & Cani, P. D. Mucus barrier, mucins and gut microbiota: the expected slimy partners? *Gut* **69**, 2232 (2020).
51. Aust, D. E. *et al.* Altered distribution of β-catenin, and its binding proteins E-cadherin and APC, in ulcerative colitis-related colorectal cancers. *Modern Pathology* **14**, 29–39 (2001).
52. Winton, D. J. & Ponder, B. A. J. Stem-cell organization in mouse small intestine. *Proc Biol Sci* **241**, 13–18 (1990).
53. Winawer, S. J. *et al.* Colorectal Cancer Screening: Clinical Guidelines and Rationale The Adenoma-Carcinoma Sequence. *Gastroenterology* **112**, 594–642 (1997).
54. Gillen, C. D., Walmsley, R. S., Prior, P., Andrews, H. A. & Allan, R. N. Ulcerative colitis and Crohn's disease: a comparison of the colorectal cancer risk in extensive colitis. *Gut* **35**, 1590 (1994).
55. Pizarro, T. T. *et al.* Challenges in IBD Research: Preclinical Human IBD Mechanisms. *Inflamm Bowel Dis* **25**, S5–S12 (2019).
56. Heller, C. A. *et al.* Challenges in IBD Research. *Inflamm Bowel Dis* **25**, S31–S39 (2019).
57. Kim, H. J., Huh, D., Hamilton, G. & Ingber, D. E. Human gut-on-a-chip inhabited by microbial flora that experiences intestinal peristalsis-like motions and flow. *Lab Chip* **12**, 2165–2174 (2012).

595 **Figure Legends**

596 **Figure 1: Primary human Colon Chips generated with epithelium and fibroblasts**
597 **isolated from Healthy and IBD patient samples. A)** Photograph of the commercially available
598 Organ Chip device (left) and a cross-sectional illustration of the epithelial-stromal tissue
599 interface (right) formed with patient-derived cells, which is composed of a fibroblast rich stroma
600 that is perfused with medium to mimic interstitial fluid flow separated by a flexible, porous, ECM-
601 coated membrane from a colon epithelium above. The epithelium, which is composed of
602 absorptive cells and Goblet cells, secretes a thick mucus layer into the lumen of the apical
603 channel that also experiences fluid flow. The entire tissue-tissue interface can be stretched and
604 relaxed rhythmically to mimic peristalsis-like motions by applying cyclic suction to hollow side
605 chambers in the flexible device (not shown). **B)** Height of crypts formed in Colon Chips
606 measured at 11 days. Numbers indicate *P* values between compared groups, as determined by
607 one-way ANOVA test (n=3 Healthy, green; 2 Crohn's, magenta; and 2 UC, cyan). **C)**
608 Representative bright field microscopic images of Healthy and IBD Chips created with cells from
609 Crohn's or UC patients viewed from above on day 3, 7, and 11. A functional epithelial
610 monolayer progressively accumulated mucus, which appears as opaque blackened fuzzy
611 material, in the apical channel of all chips over the 11 day time course; however, mucus
612 accumulation was suppressed in the IBD Chips with the UC Chips displaying a greater
613 reduction (bar, 500 μm)**. D)** Brightfield image of vertical cross-sections through healthy and IBD
614 Colon chips showing that the crypt-like epithelial structures are shorter in the Crohn's and UC
615 Colon Chips (bar, 100 μm)**. E)** Histological H&E stained vertical cross-sections through healthy
616 and IBD Colon chips confirming the presence of columnar colon epithelium containing goblet
617 cells in healthy epithelium, and a significant reduction in the height of the epithelial monolayer
618 with reduced numbers of goblet cells in the IBD Chips (bar, 50 μm). **F)** Immunofluorescence
619 microscopic views showing distribution of SOX9 and CK20 in crypts in the colon epithelium of

620 Healthy and IBD Chips (bar, 50 μm). **G**) Inflammatory cytokine protein levels measured in the
621 basal outflows of Healthy (H) and IBD Chips on culture day 11 (n = 3-5 chips/ condition; chips
622 were created with cells from 3 healthy (green), 2 Crohn's (magenta), and 2 UC (cyan) patient
623 donors, with each symbol represents a chip created with cells from a different patient. Numbers
624 indicate *P* values between compared groups, as determined by two-tailed student's t-test. All
625 data represent mean ± SD; *p* values are shown in all figures.

626 **Figure 2: Peristalsis-like cyclic strain influences mucus production and fibrosis in**
627 **Colon Chips. A)** Representative side-view images microscopy of Healthy or IBD Chips with (+)
628 and without (-) exposure to mechanical deformations visualizing mucus layer accumulation
629 (white diffuse material) in Healthy Chips using dark-field microscopy. Note that limited mucus
630 was produced by IBD epithelium (bar, 1 mm). **B)** Quantification of the height of the mucus layer
631 overlying Healthy and IBD epithelium on-chip when cultured under the conditions in A. Numbers
632 indicate *P* values between compared groups, as determined by one-way ANOVA test. (n = 4
633 healthy, green; 2 Crohn's, magenta; and 2 UC, cyan). **C)** Heat map of genes showing that
634 peristalsis-like mechanical stimulation (+) increases expression of genes related to mucus
635 production in Healthy Chips, but not IBD Chips (n = 3 healthy, 1 Crohn's and 2 UC). **D)** Second
636 harmonic microscopic images of the fibroblast stroma in Healthy versus IBD Chips showing
637 greater collagen fibril accumulation (green) with mechanical strain (+ Strain) in both chips, and
638 that this response is greatly accentuated in IBD Chips (bar, 200 μm). **E)** Collagen fibril signal
639 intensity in the stroma of Healthy versus IBD Chips quantified in second harmonic microscopic
640 images. Numbers indicate *P* values between compared groups, as determined by one-way
641 ANOVA test (n = 3 healthy, green; 2 Crohn's, magenta; and 2 UC, cyan). **F)** Heat map of genes
642 showing that peristalsis-like cyclic strain enhances expression of genes associated with fibrillar
643 collagen production in IBD fibroblasts, but not in healthy fibroblasts (n = 3 healthy, 1 Crohn's
644 and 2 UC). **G)** Heat maps of showing that cyclic strain enhances greater expression of IBD-

645 associated inflammatory genes in IBD Chips compared to Healthy Chips both in epithelium and
646 fibroblasts (n=3 Healthy, 1 Crohn's, and 2 UC).

647 **Figure 3: Effects of ovarian hormones in Female Colon Chips. A)** Production of pro-
648 inflammatory cytokine and chemokine proteins in Apical and Basal channels of Healthy versus
649 IBD Chips 7 days post treatment with different female hormone exposures (E2, P4, and PAHs,
650 as indicated). Note that exposure to female hormones significantly increased expression of
651 inflammatory factors in both epithelium and fibroblast of IBD Colon Chips whereas they
652 suppressed their production in Healthy Chips. **B)** Collagen fibril signal intensity in the stroma of
653 Healthy versus IBD Chips quantified in second harmonic microscopic images showing that only
654 exposure to pregnancy-like hormonal conditions produced a major increase in stromal
655 fibrillogenesis, and this only was observed in IBD fibroblasts and not healthy fibroblasts from
656 IBD patients. Numbers indicate *P* values between compared groups, as determined by one-way
657 ANOVA test (n=4-6 chips of 1 Crohn's and 1 Healthy patients from 2 independent experiments).
658 **C)** Second harmonic microscopic images of fibrillar collagen (green) produced by fibroblasts
659 showing that the E2 + E4 produce a small increase in fibrillogenesis in IBD Chips, while
660 simulating pregnancy by exposure to E2 + E4 + PAH results in dramatic collagen fibril
661 accumulation, and that neither of these responess are observed in Healthy Chips (bar, 200 μm;
662 n=4-6 chips of 1 Crohn's and 1 Healthy patients from 2 independent experiments).

663 **Figure 4: Tissue recombinant chips reveal that the IBD fibroblasts drive**
664 **compromise of the permeability barrier and inflammation in the epithelium**. **A)** Graphs
665 showing that intestinal barrier permeability to cascade blue is much higher in homotypic IBD
666 Chips compared to Healthy Chips and that tissue recombinants of IBD fibroblasts with healthy
667 (H) epithelium results in a similar high level of barrier compromise on-chip. This is not observed
668 in the IBD or healthy epithelium in the absence of fibroblasts or in IBD epithelium with healthy
669 fibroblasts. Numbers indicate *P* values between compared groups, as determined by one-way
670 ANOVA test (n = 3 healthy, green; 2 Crohn's, magenta; and 2 UC, cyan). **B)** Quantification of

671 cytokine protein levels revealed that combination of IBD fibroblasts with healthy epithelium
672 results in increased production of IL-6 and MCP-1 in Colon Chips, whereas this was not seen in
673 healthy epithelium alone or homotypic Colon Chips. Numbers indicate *P* values between
674 compared groups, as determined by one-way ANOVA test (n = 3 healthy, green; 1 Crohn's,
675 magenta; and 2 UC, cyan). **C)** IL-6 and MCP-1 production by IBD epithelium also required the
676 presence of IBD fibroblasts. Numbers indicate *P* values between compared groups, as
677 determined by one-way ANOVA test (n = 3 healthy, green; 1 Crohn's, magenta; and 2 UC,
678 cyan). **D)** Peristalsis-like cyclic strain preferentially stimulates migration of PBMCs (magenta)
679 from the fibroblast stroma in the basal channel (Basal) to the epithelium in the apical channel
680 (Apical) in IBD Chips but not in heterotypic chips with IBD epithelium and healthy fibroblasts or
681 in Healthy Chips. **E)** Quantification of the results from **D** confirmed that IBD Chips exhibited
682 higher baseline recruitment of PBMCs to the surface of the fibroblast stroma in the basal
683 channel and that this was not altered by mechanical strain, whereas IBD epithelium combined
684 with healthy stroma or Healthy Chips only displayed significantly less PBMC recruitment. In
685 contrast, the number of PBMCs that migrated to the epithelium in the Apical channel more than
686 doubled in IBD Chips when they were exposed to peristalsis-like mechanical deformations, and
687 overall migration of PBMCs was minimal when IBD fibroblasts were absent. Numbers indicate
688 *P* values between compared groups, as determined by one-way ANOVA test (n = 2 healthy,
689 green; 1 Crohn's, magenta; and 1 UC, cyan).

690 **Figure 5: Exposure to carcinogen preferentially promotes mutagenesis and early**
691 **steps in carcinogenesis in IBD Chips. A)** DIC images of the epithelium when viewed from
692 above in Healthy (H) and IBD Chips after 21 days of culture in the presence or absence of the
693 carcinogen (ENU) showing that undulating crypt-like structures are lost in both Healthy and IBD
694 Chips after exposure to ENU (bar, 500 μm). **B)** Quantification of results from **A** showing that
695 ENU decreases height of the epithelium in both healthy and IBD Colon Chips. Numbers indicate
696 *P* values between compared groups, as determined by one-way ANOVA test (n = 4 healthy,

697 green; 2 Crohn's, magenta; and 2 UC, cyan). **C)** Epithelial barrier permeability increased as a
698 result of exposure to ENU in Healthy and IBD Chips. Numbers indicate *P* values between
699 compared groups, as determined by one-way ANOVA test. (n = 3 healthy, green; 2 Crohn's,
700 magenta; and 2 UC, cyan). **D)** Heatmaps showing inflammatory cytokine protein levels
701 measured in outflows from the apical channel of Healthy and IBD Chips 3 weeks post-ENU
702 exposure. Importantly, ENU exposure significantly increased inflammatory cytokine production
703 in IBD Chips made with cells from both Crohn's and UC patients compared to healthy patients.
704 **E)** Confocal microscopic top-view images showing β-catenin and E-cadherin localization and
705 nuclear staining (DAPI) in the epithelium within Healthy and IBD Chips 3 weeks post-ENU
706 exposure (bar, 20 μm). **F)** Quantification of protein staining intensity and morphology reveal that
707 ENU exposure decreases E-cadherin levels and increases nuclear localization of β-catenin in
708 IBD patient-derived Colon Chips compared to Healthy Chips. ENU exposure also resulted in
709 greater nucleus size and less roundness. Numbers indicate *P* values between compared
710 groups, as determined by Student's t-test (n = 3 healthy, green; 2 Crohn's, magenta; and 2 UC,
711 cyan). **G)** Plots showing copy number changes across all human chromosomes in Healthy and
712 IBD Chips pre- (red) and 3 weeks post-ENU exposure (blue). Green bars indicate amplification
713 of gene sequences for the whole chromosome. Each symbol represents an individual Healthy or
714 IBD patient-derived chip.

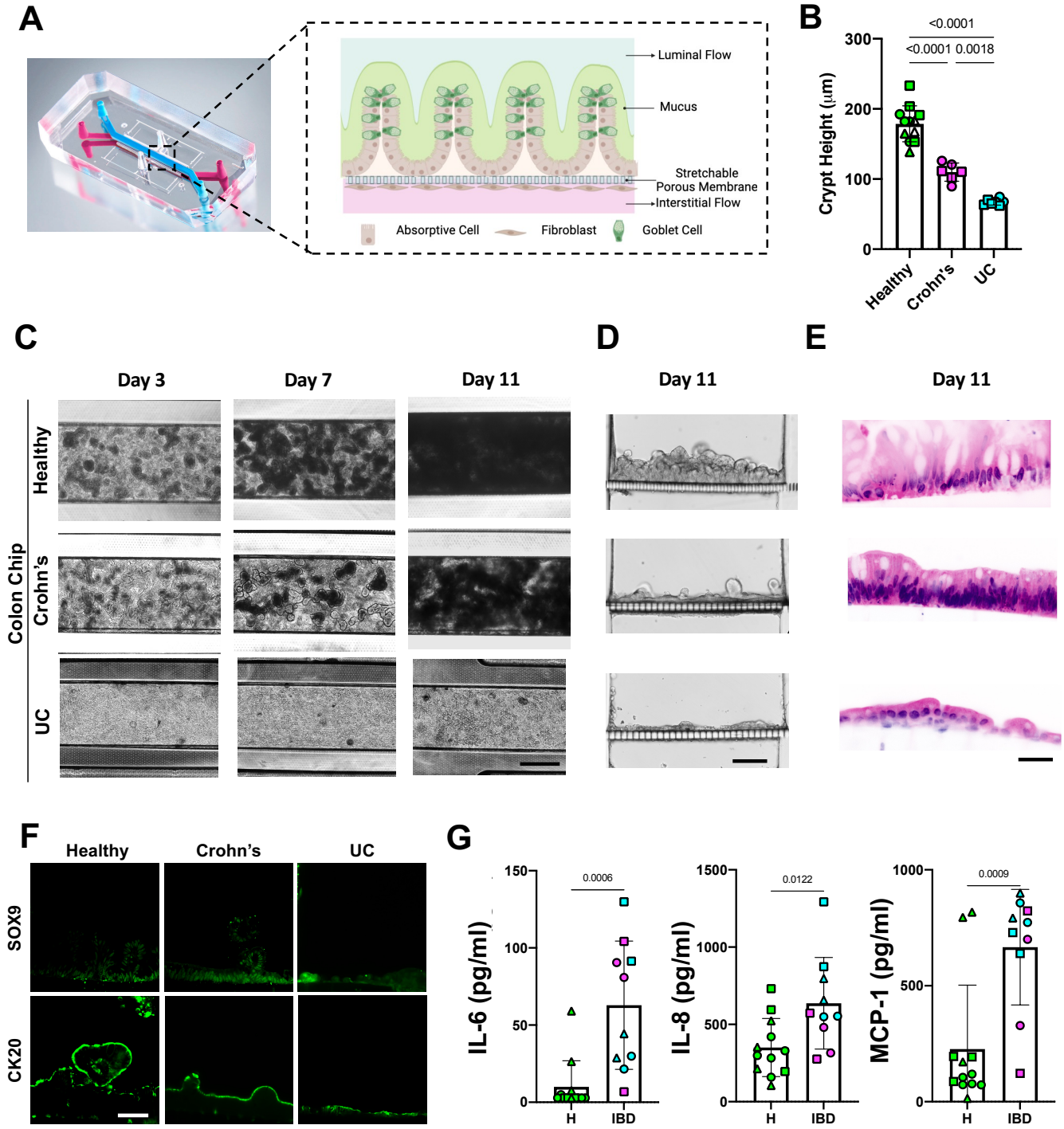
A
Luminal Flow
Mucus
Stretchable Porous Membrane
Interstitial Flow
Absorptive Cell
Fibroblast
Goblet Cell
B
<0.0001
<0.0001
0.0018
Crypt Height (μm)
300
200
100
0
Healthy
Crohn's
UC
C
Day 3
Day 7
Day 11
Colon Chip
Healthy
Crohn's
UC
D
Day 11
E
Day 11
F
Healthy
Crohn's
UC
SOX9
CK20
G
IL-6 (pg/ml)
0.0006
150
100
50
0
H
IBD
IL-8 (pg/ml)
0.0122
1500
1000
500
0
H
IBD
MCP-1 (pg/ml)
0.0009
1000
500
0
H
IBD

Fig. 1

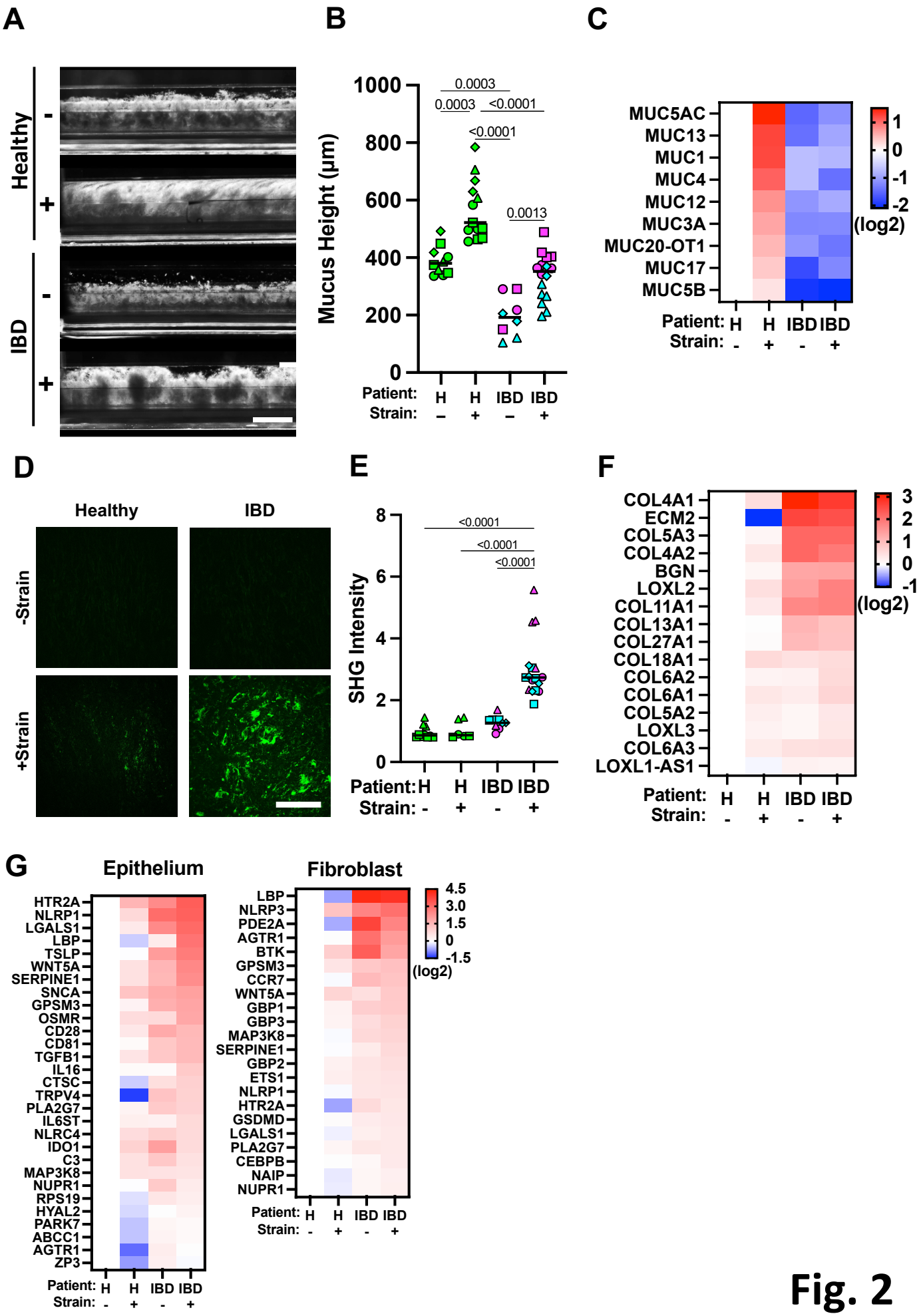
A
Healthy
-
+
IBD
-
+
B
Mucus Height (µm)
1000
800
600
400
200
0
0.0003
0.0003
<0.0001
<0.0001
0.0013
Patient: H H IBD IBD
Strain: – + – +
C
MUC5AC
MUC13
MUC1
MUC4
MUC12
MUC3A
MUC20-OT1
MUC17
MUC5B
1
0
-1
-2
(log2)
Patient: H H IBD IBD
Strain: - + - +
D
Healthy
IBD
-Strain
+Strain
E
SHG Intensity
8
6
4
2
0
<0.0001
<0.0001
<0.0001
Patient: H H IBD IBD
Strain: - + - +
F
COL4A1
ECM2
COL5A3
COL4A2
BGN
LOXL2
COL11A1
COL13A1
COL27A1
COL18A1
COL6A2
COL6A1
COL5A2
LOXL3
COL6A3
LOXL1-AS1
3
2
1
0
-1
(log2)
Patient: H H IBD IBD
Strain: - + - +
G
Epithelium
HTR2A
NLRP1
LGALS1
LBP
TSLP
WNT5A
SERPINE1
SNCA
GPSM3
OSMR
CD28
CD81
TGFB1
IL16
CTSC
TRPV4
PLA2G7
IL6ST
NLRC4
IDO1
C3
MAP3K8
NUPR1
RPS19
HYAL2
PARK7
ABCC1
AGTR1
ZP3
Patient: H H IBD IBD
Strain: - + - +
Fibroblast
LBP
NLRP3
PDE2A
AGTR1
BTK
GPSM3
CCR7
WNT5A
GBP1
GBP3
MAP3K8
SERPINE1
GBP2
ETS1
NLRP1
HTR2A
GSDMD
LGALS1
PLA2G7
CEBPB
NAIP
NUPR1
4.5
3.0
1.5
0
-1.5
(log2)
Patient: H H IBD IBD
Strain: - + - +

Fig. 2

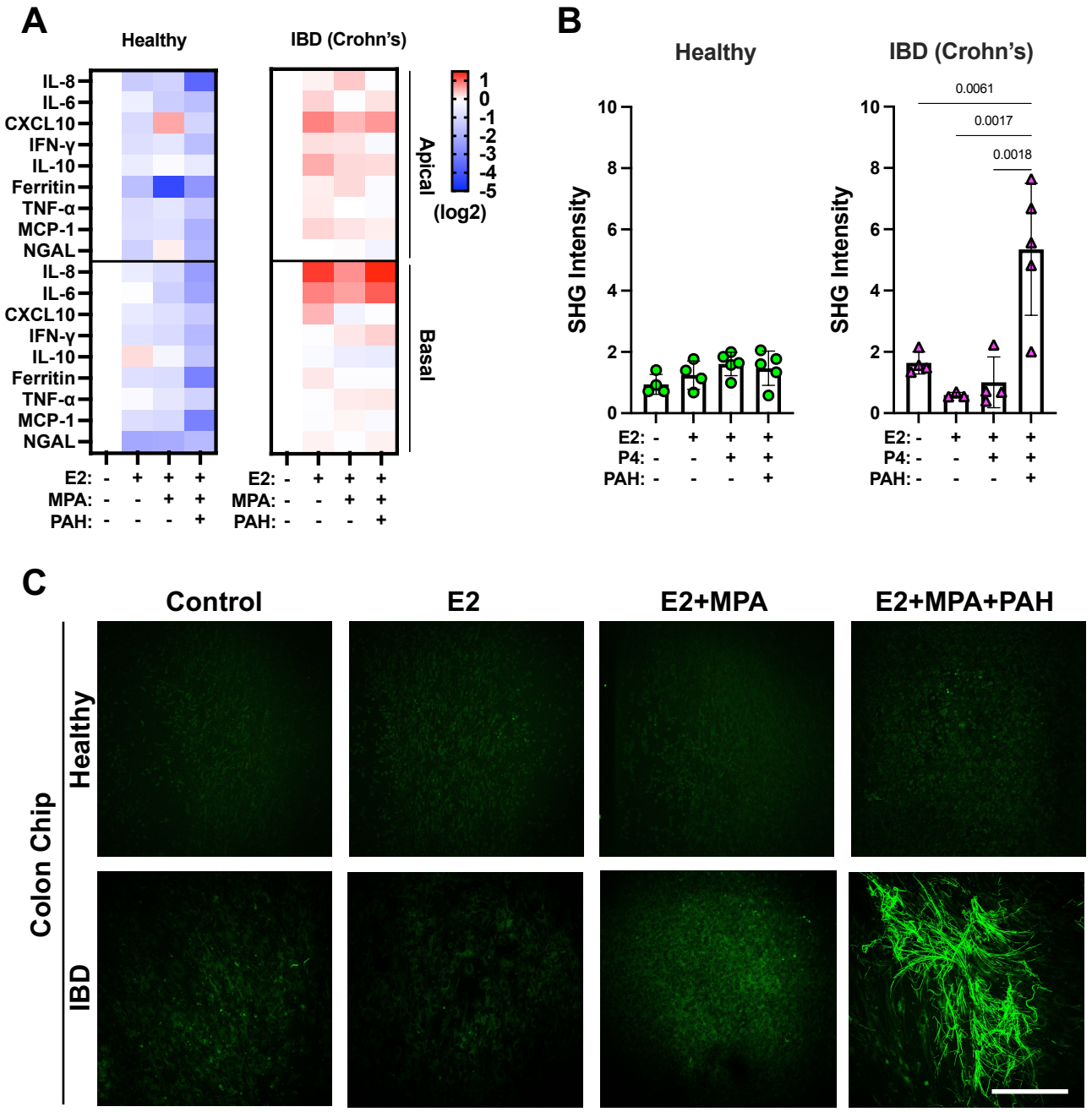
A
Healthy
IBD (Crohn's)
IL-8
IL-6
CXCL10
IFN-γ
IL-10
Ferritin
TNF-α
MCP-1
NGAL
Apical
Basal
1
0
-1
-2
-3
-4
-5
(log2)
E2:
MPA:
PAH:
B
Healthy
IBD (Crohn's)
SHG Intensity
0.0061
0.0017
0.0018
E2:
P4:
PAH:
C
Control
E2
E2+MPA
E2+MPA+PAH
Colon Chip
Healthy
IBD

Fig. 3

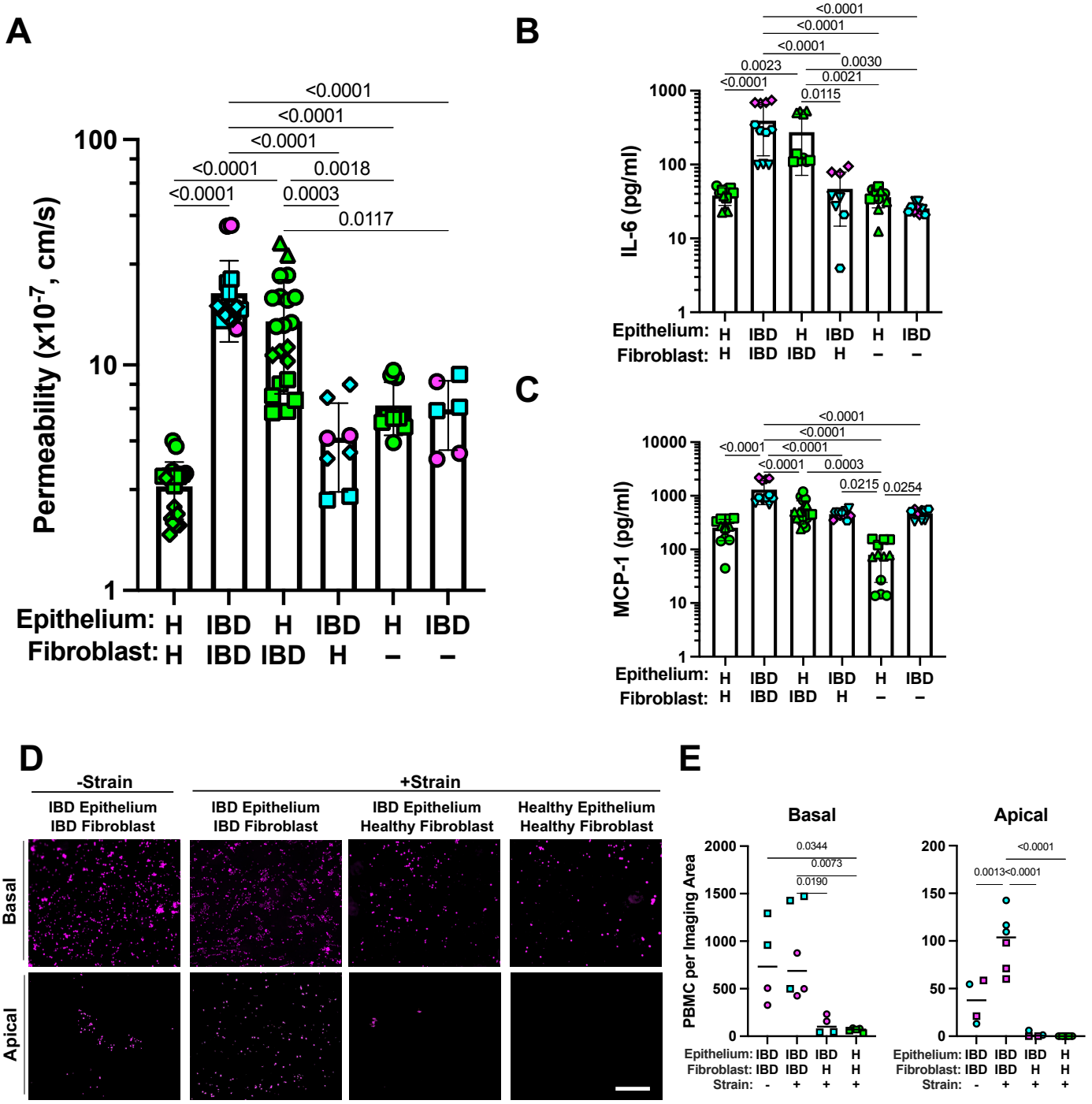
A
Permeability (x10-7, cm/s)
100
10
1
<0.0001
<0.0001
<0.0001
<0.0001
0.0018
<0.0001
0.0003
0.0117
Epithelium: H IBD H IBD H IBD
Fibroblast: H IBD IBD H – –
B
IL-6 (pg/ml)
1000
100
10
1
<0.0001
<0.0001
<0.0001
0.0023
0.0030
<0.0001
0.0021
0.0115
Epithelium: H IBD H IBD H IBD
Fibroblast: H IBD IBD H – –
C
MCP-1 (pg/ml)
10000
1000
100
10
1
<0.0001
<0.0001
<0.0001
<0.0001
<0.0001
0.0003
0.0215
0.0254
Epithelium: H IBD H IBD H IBD
Fibroblast: H IBD IBD H – –
D
-Strain
+Strain
IBD Epithelium IBD Fibroblast
IBD Epithelium IBD Fibroblast
IBD Epithelium Healthy Fibroblast
Healthy Epithelium Healthy Fibroblast
Basal
Apical
E
Basal
Apical
PBMC per Imaging Area
2000
1500
1000
500
0
0.0344
0.0073
0.0190
200
150
100
50
0
0.0013
<0.0001
<0.0001
Epithelium: IBD IBD IBD H
Fibroblast: IBD IBD H H
Strain: - + + +

Fig. 4

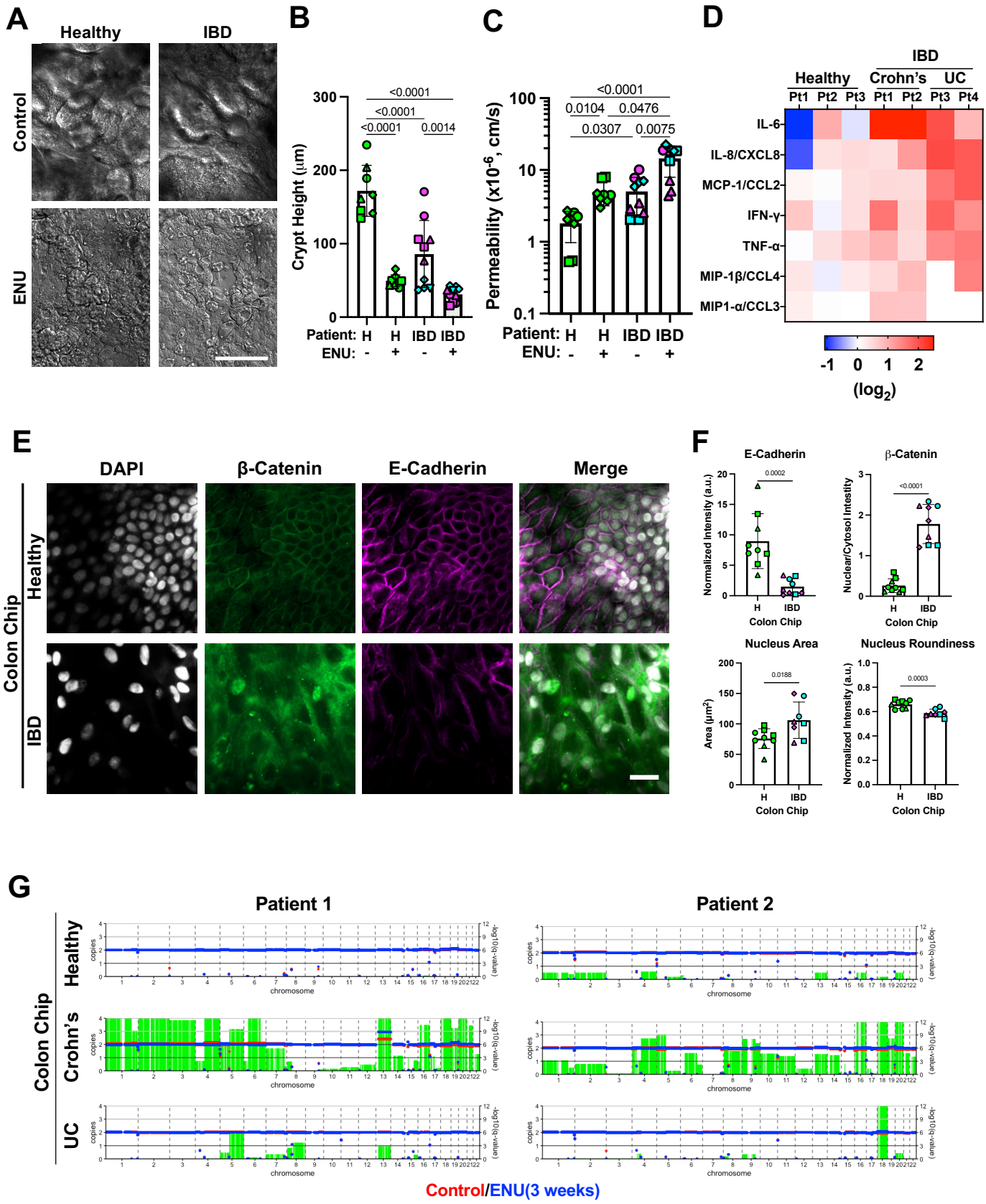
A
Healthy
IBD
Control
ENU
B
Crypt Height (μm)
<0.0001
<0.0001
<0.0001
0.0014
Patient: H H IBD IBD
ENU: - + - +
C
Permeability (x10-6, cm/s)
<0.0001
0.0104
0.0476
0.0307
0.0075
Patient: H H IBD IBD
ENU: - + - +
D
IBD
Healthy
Crohn's
UC
Pt1 Pt2 Pt3 Pt1 Pt2 Pt3 Pt4
IL-6
IL-8/CXCL8
MCP-1/CCL2
IFN-γ
TNF-α
MIP-1β/CCL4
MIP1-α/CCL3
-1 0 1 2
(log2)
E
DAPI
β-Catenin
E-Cadherin
Merge
Colon Chip
Healthy
IBD
F
E-Cadherin
0.0002
Normalized Intensity (a.u.)
β-Catenin
<0.0001
Nuclear/Cytosol Intestity
H IBD
Colon Chip
Nucleus Area
0.0188
Area (μm2)
Nucleus Roundiness
0.0003
Normalized Intensity (a.u.)
G
Patient 1
Patient 2
Colon Chip
Healthy
Crohn's
UC
copies
chromosome
-log10(q-value)
Control/ENU(3 weeks)

Fig. 5

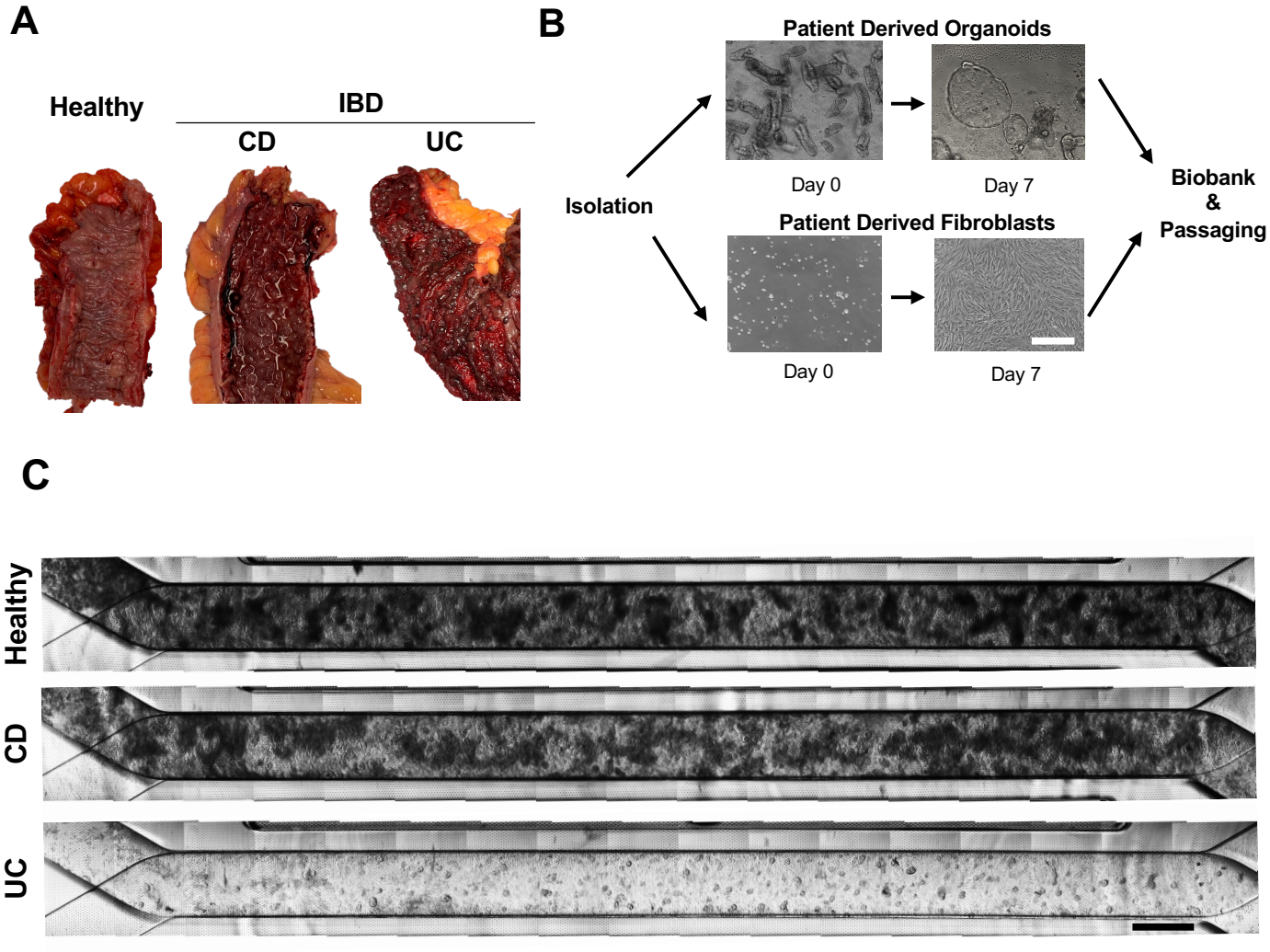

Extended Data Fig. 1

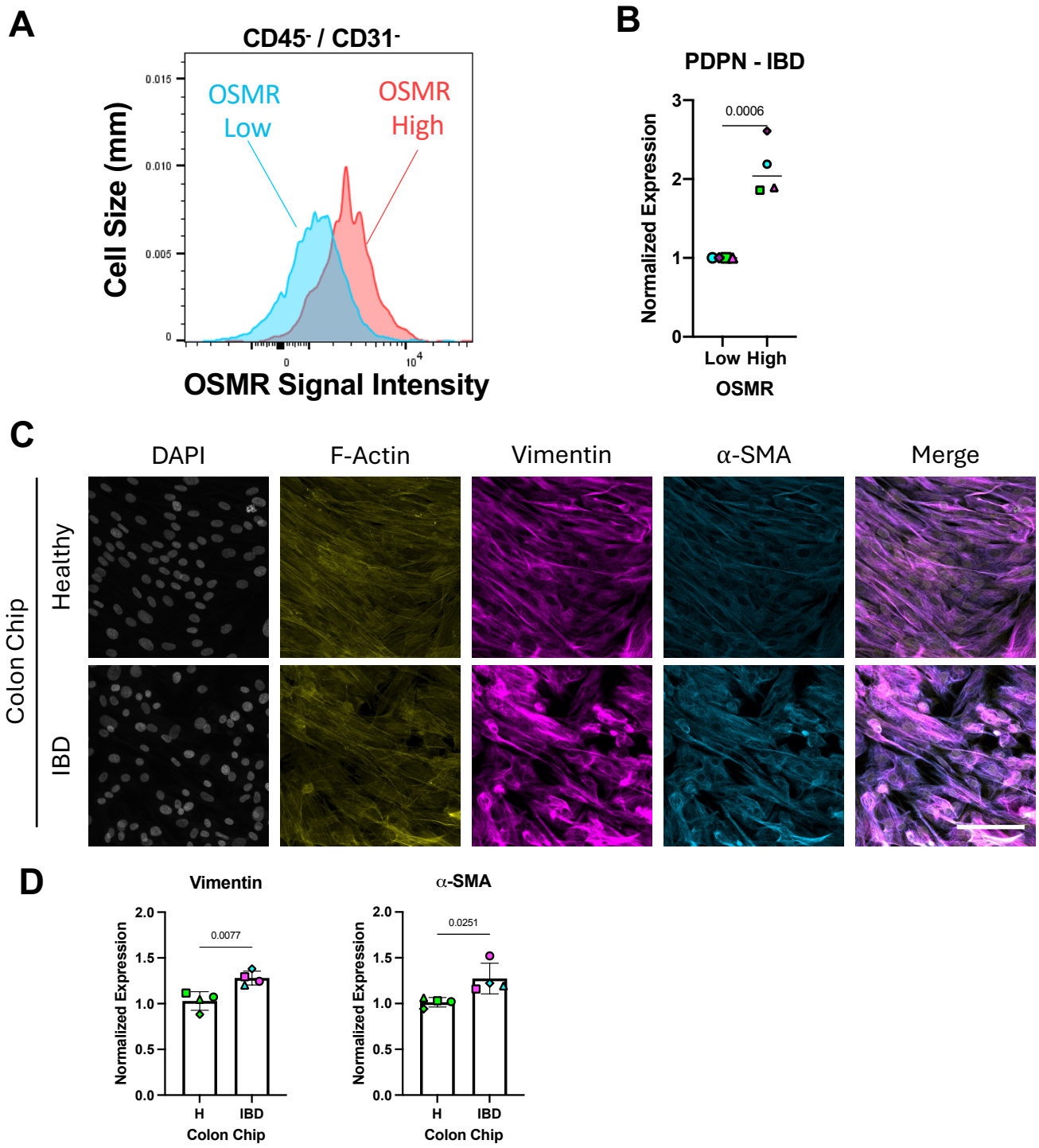

Extended Data Fig. 2

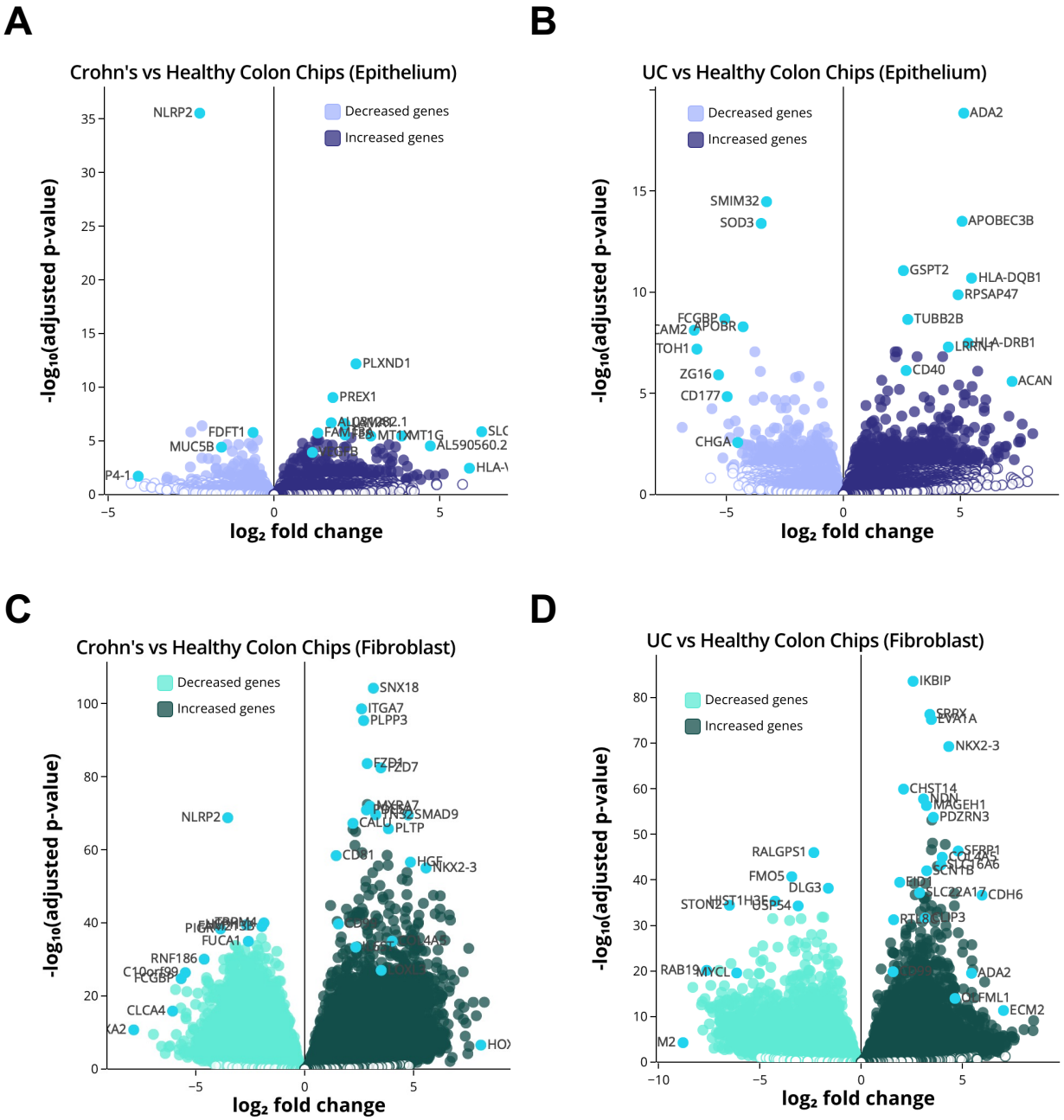

Extended Data Fig. 3

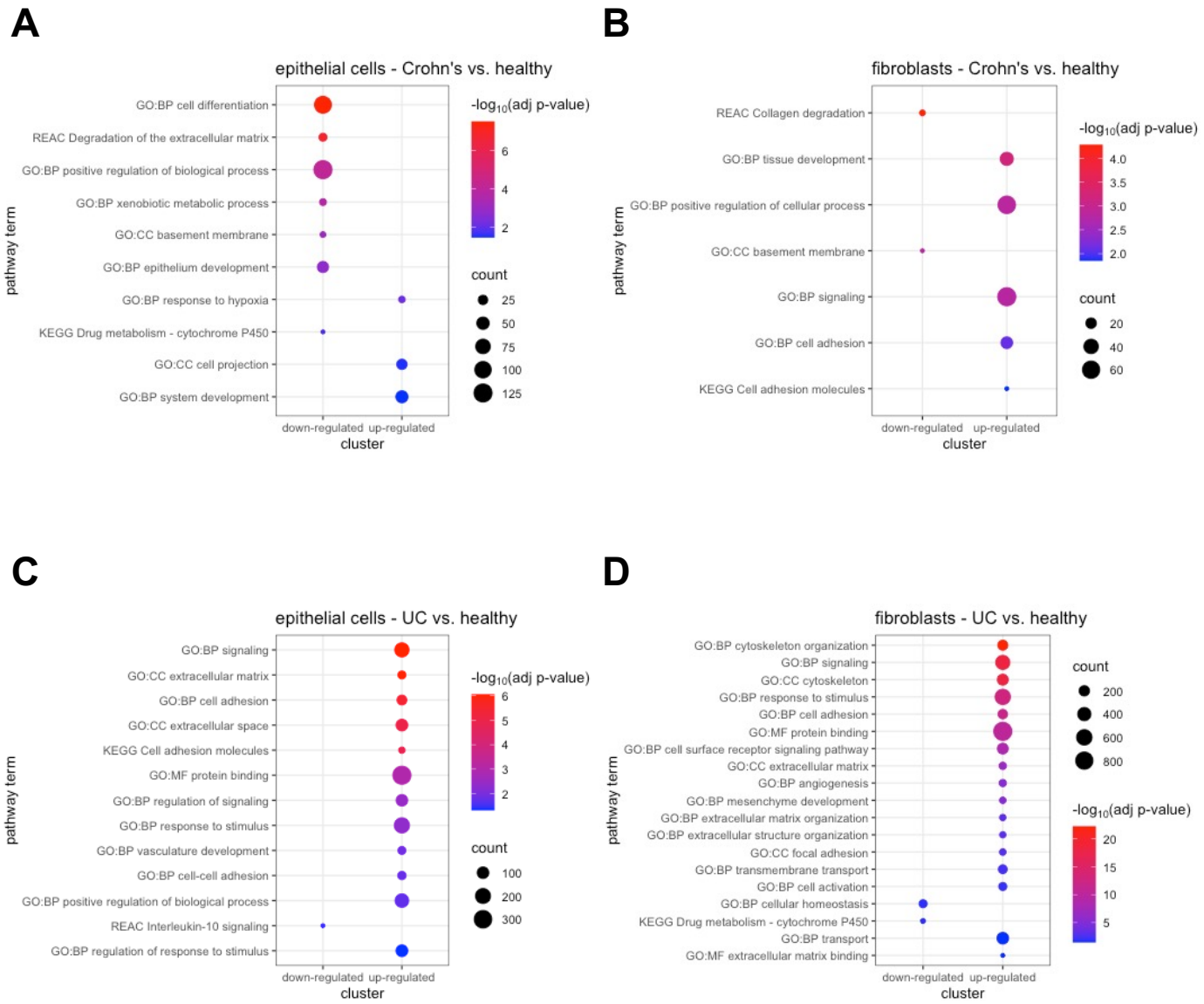

Extended Data Fig. 4

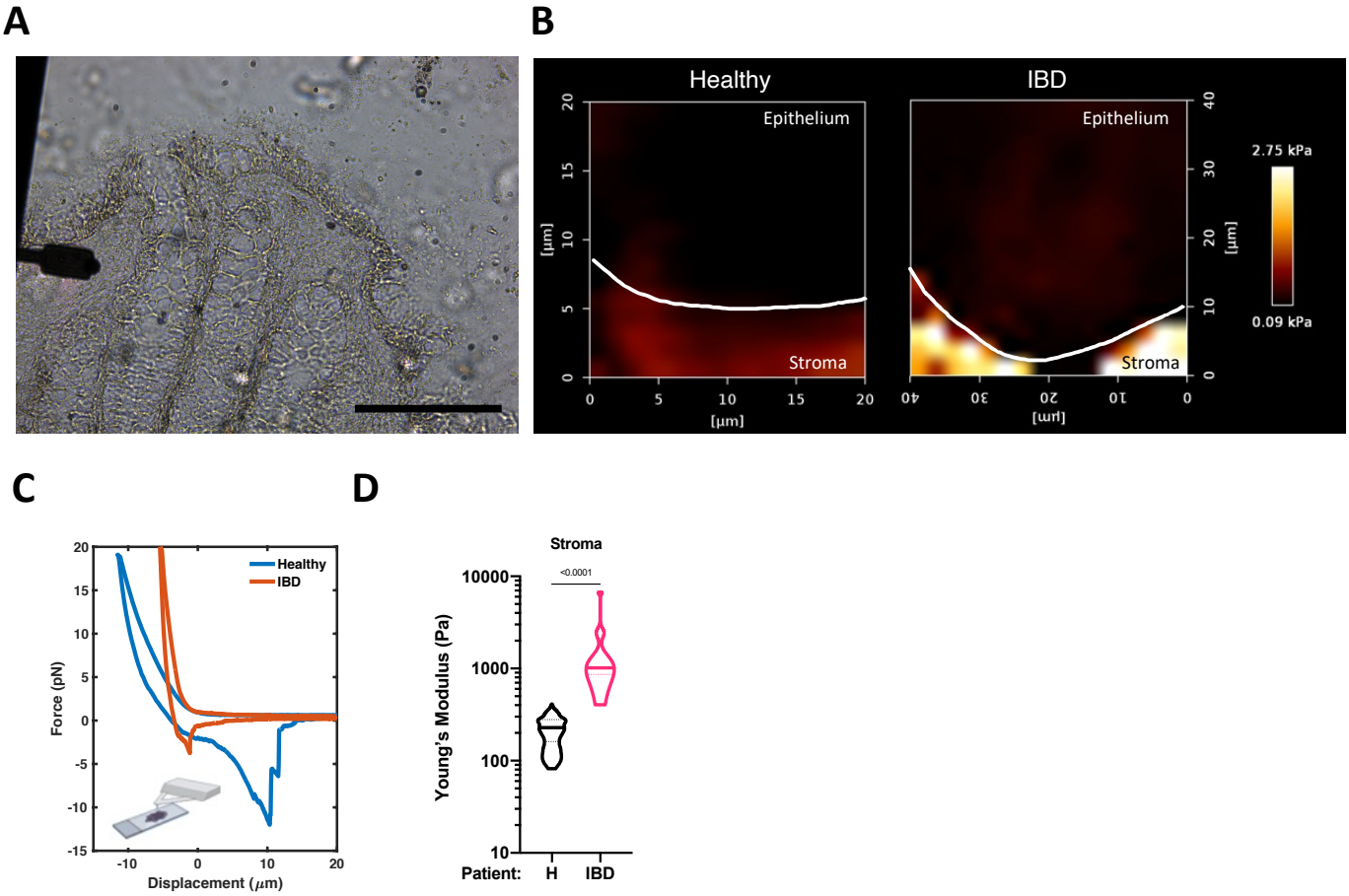

Extended Data Fig. 5

A

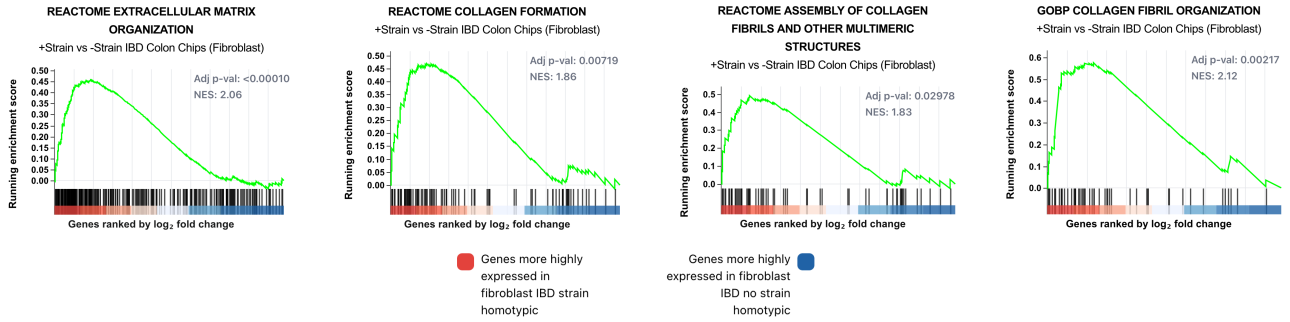

B

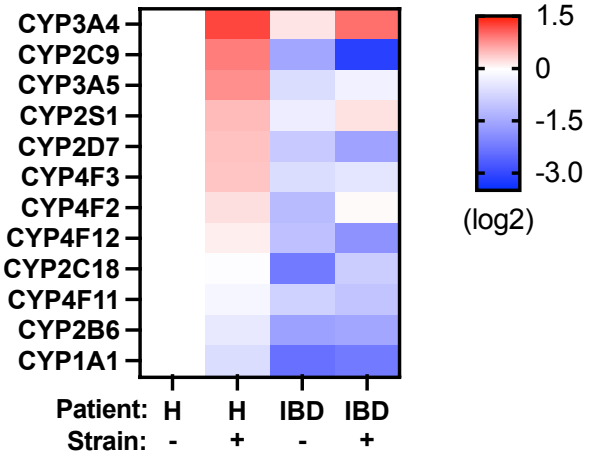

Extended Data Fig. 6

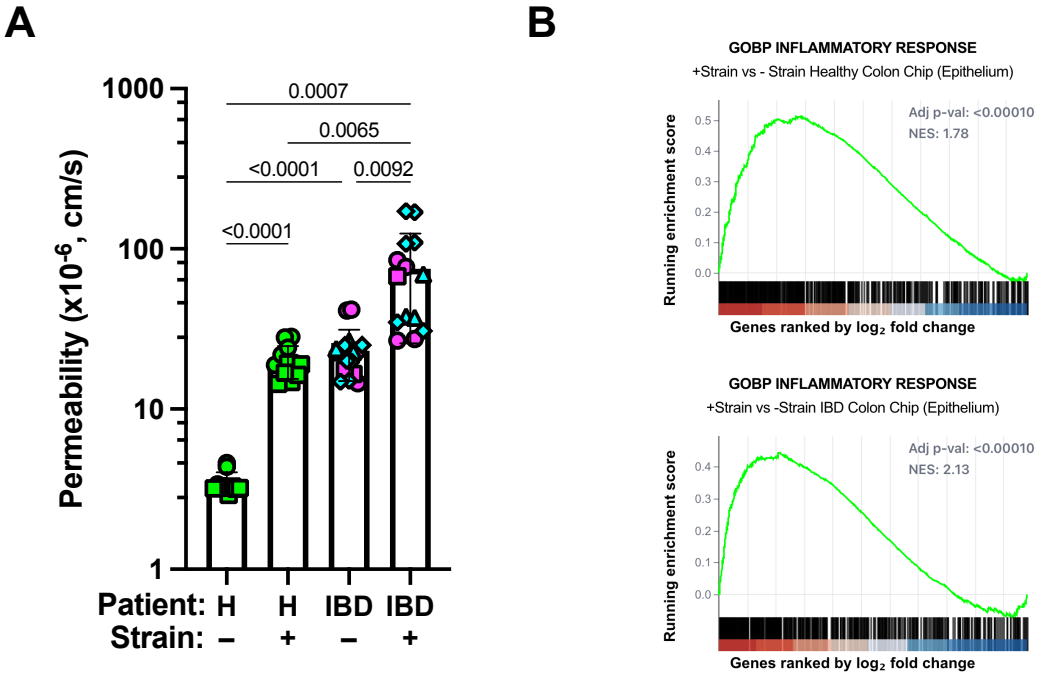

Extended Data Fig. 7

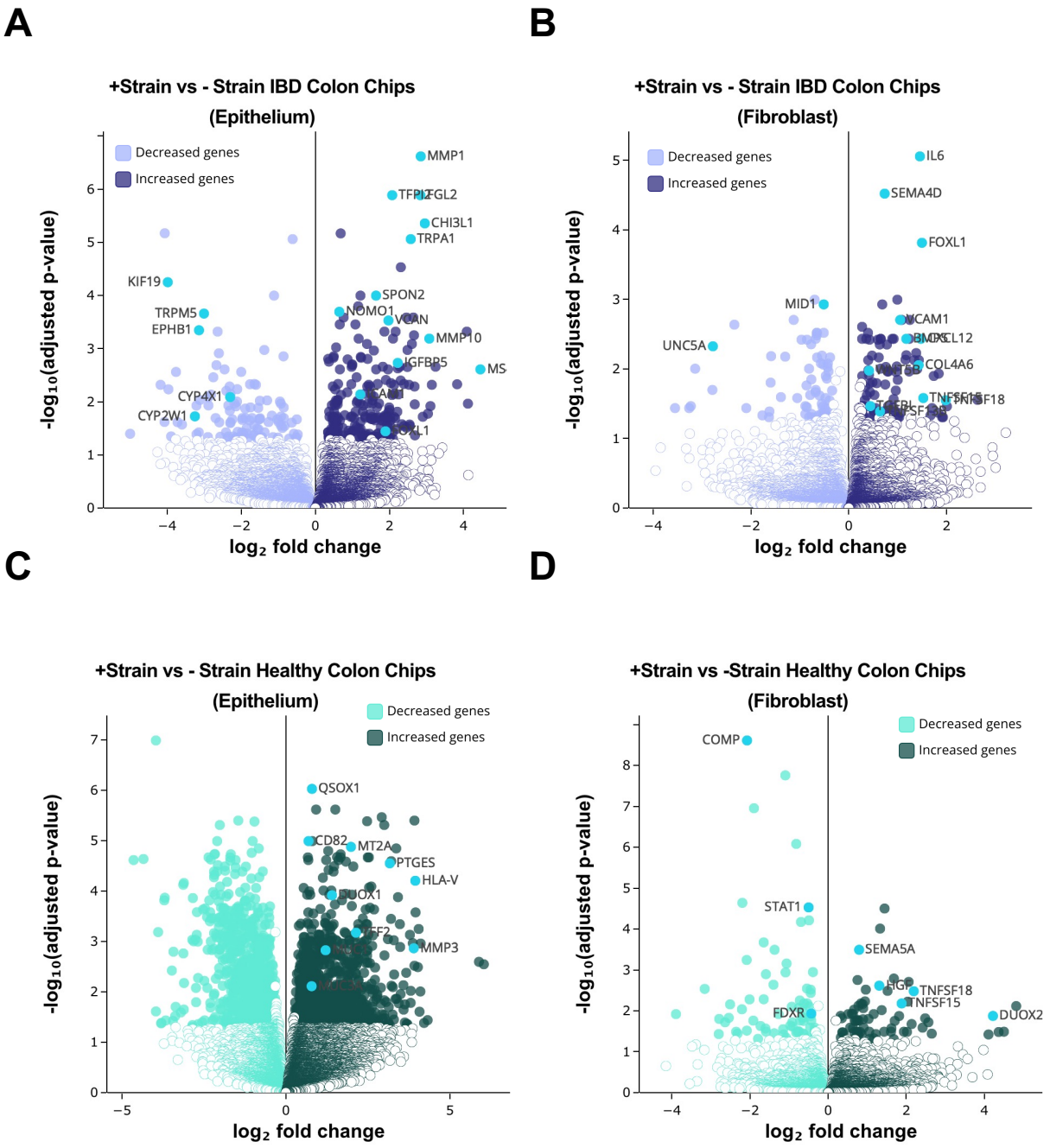

Extended Data Fig. 8

A

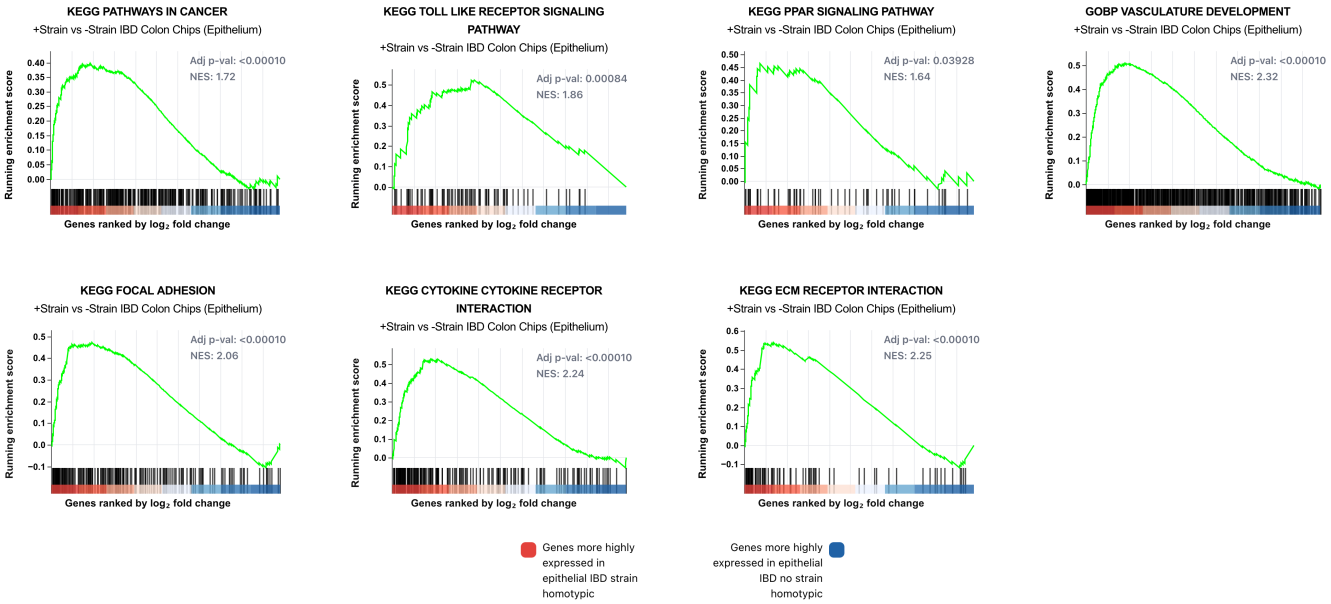

B

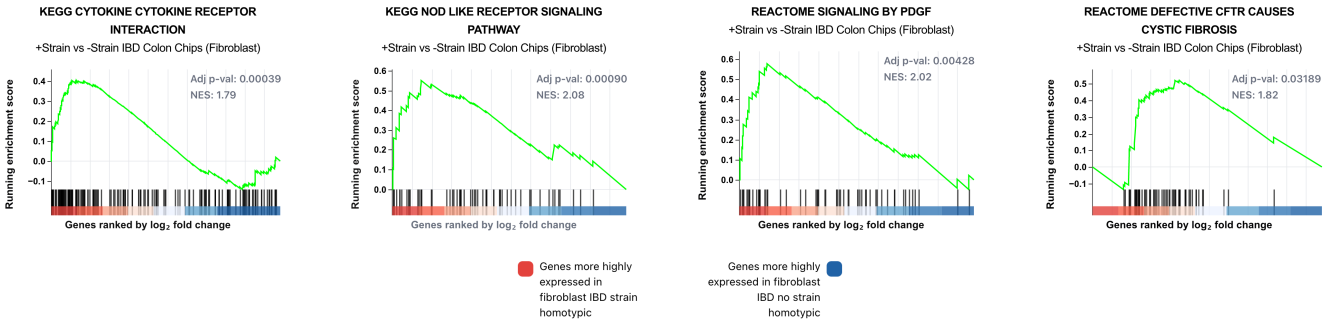

Extended Data Fig. 9

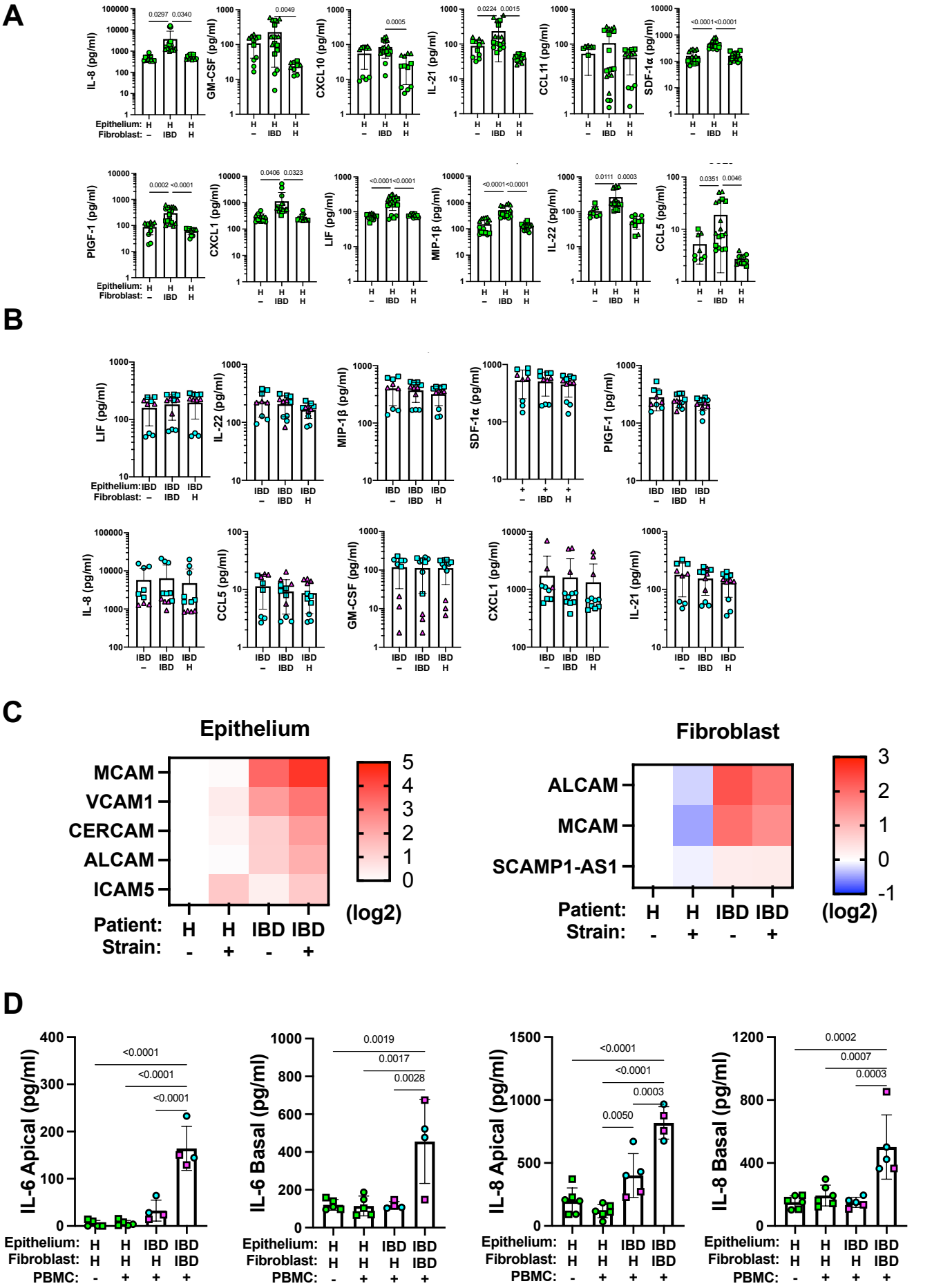

Extended Data Fig. 10